Quantitative proteomic analysis of the central amygdala in neuropathic pain model rats

Kersti Karu[1], Richard S. Swanwick[1], Amparo Novejarque-Gadea[2], Ana Antunes-Martins[3], Benjamin Thomas[6], Eiji Yoshimi[1], William Foster[1], Min Fang[4], Stephen B. McMahon[3], David L.H. Bennett[5], Andrew S.C. Rice[2], and Kenji Okuse*[1]

[1]Department of Life Sciences, Faculty of Natural Sciences, Imperial College London, London SW7 2AZ, U.K.
[2]Department of Surgery and Cancer, Faculty of Medicine, Imperial College London, London SW10 9NH, U.K.
[3]The Wolfson Centre for Age-Related Diseases, King's College London, Guy's Campus, London SE1 1UL, U.K.
[4]Public Health England, London SE1 8UG, U.K.
[5]Nuffield Department of Clinical Neurosciences, University of Oxford, Oxford OX3 9DU, U.K.
[6]Central Proteomics Facility, Sir William Dunn School of Pathology, University of Oxford, Oxford, UK

* Corresponding author (KO): E-mail: k.okuse@imperial.ac.uk, Phone: +44-0207-5945742

Abstract

Pain and emotional distress have a reciprocal relation. The amygdala has been implicated in emotional processing. The central nucleus of amygdala (CeA) receives nociceptive information from the dorsal horn of spinal cord, and responsible for the central plasticity in chronic pain. Neuropathic pain is a type of severe chronic pain and can be strongly influenced by emotional components. Plastic changes in CeA may play a key role in the development and/or maintenance of neuropathic pain. We studied the expression levels of proteins in CeA of spinal nerve transection (SNT) model rats. Total tissue lysate proteins were separated by two dimensional-gel electrophoresis (2D-PAGE). Gels from different time points were compared using Progenesis SameSpot software, and the spots with Fold Change greater than 2 were excised for the protein identification by mass spectrometry. We identified more than 50 cytosolic proteins as significantly altered in their expressions in CeA of SNT rats, and most of these changes have been validated at mRNA levels by qRT-PCR. We also identified more than 40 membrane proteins as notably up- or down-regulated in CeA of SNT model rats relative to a control using stable isotope dimethyl labeling nano-LC-MS/MS based proteomics and found that one of such protein, doublecortin (DCX), a microtubule-associated protein expressed by neuronal precursor cells during development, is specifically localized in the membrane fraction without changes in total amount of the protein. Immunohistochemistry showed that doublecortin is expressed in processes in CeA of

rats 7 and 21 days post SNT surgery, suggesting doublecortin is one of the proteins which may contribute to the plastic changes, namely re-development or re-wiring of neural networks, in CeA in the neuropathic pain model. These dysregulated proteins may play roles in reciprocal relationships between pain and psychological distress in the amygdala and contribute to central sensitization.

Key words: amygdala, neuropathic pain, proteomic, mass spectrometry, spinal nerve transection (SNT), LC-MS/MS, stable isotope dimethyl labelling.

Introduction

Pain has a profound impact on the level of emotional distress, and psychological states play an important role in determining the extent of pain. Thus the relationship between pain and psychological distress such as depression and anxiety appears to be reciprocal. The amygdala is a structure in the brain located in the anterior inferior temporal lobe, and has been implicated in emotional processing. The amygdala can be divided into anatomically and functionally distinct nuclei, namely basal, lateral, medial, and central nucleus. Among them, the central nucleus of amygdala (CeA) serves as the output nucleus for major amygdala functions, while other nuclei are involved in receiving input from the sensory systems, the sense of smell and pheromone-processing, and emotional arousal. The capsular part of the CeA is defined as nociceptive amygdala, because it receives nociceptive information from the dorsal horn of spinal cord

Neuropathic pain is a type of severe chronic pain which is generally refractive to treatment. Although neuropathic pain is defined as pain caused by a lesion or disease somatosensory nervous system, it can also be strongly influenced by emotional components. Neuropathic pain is associated with plastic changes in both peripheral and central nervous system [1]. Neural plasticity includes changes in biochemical profile, function, and structure of neurons. CeA is thought to be one of the key areas responsible for the central plasticity in chronic pain including neuropathic pain, because CeA integrates nociceptive input from the spinal cord and polymodal information

from the thalamus and cortex. In fact, CeA has been found to exhibit a high degree of plasticity in chronic pain models. The immediate-early gene, c-Fos and metabotropic glutamate receptors have been found to be upregulated in CeA in chronic pain conditions [2, 3]. The excitability of CeA neurons has also been found to be increased in rats with neuropathic pain [4] and arthritic pain [1, 5] conditions. These plastic changes in CeA may play a key role in the development and/or maintenance of chronic pain, however little is known about the regulation of cell proliferation and differentiation in the amygdala in response to neuropathic pain. Only a few studies have actually examined amygdala in depth at the proteome level [6-8].

Transcriptomics or genetic analysis provides a partial view of the signaling pathways driving neuropathic pain response because of their limited capacity to predict concentrations changes at the proteins level or inform about status of protein changes [9, 10]. Mass spectrometry (MS)-based proteomics analysis of the central amygdala proteins that changes in response to the spinal nerve transection (SNT) may have a large potential to unveil novel signaling mechanisms of clinical relevance [9, 11]. Quantitative proteomics further enable to identify the altered expression of proteins. One of the most utilised approaches in proteomics to identify differential proteins in complex samples is isoelectric focusing two dimensional polyacrylamide gel electrophoresis (2D-PAGE)-based MS [12, 13]. The silver stained spots between different gels are compared using spot matching software alignments. The differential 2D-PAGE spots are excised, in-gel digested with an enzyme and the resulting peptides are separated on the LC column prior to mass spectrometry analysis. Another approach is to use two-dimensional difference gel electrophoresis which requires an extra step to pre-label proteins with fluorescent dyes before isoelectric focusing (2D-DIGE). By using different dyes on 2D-DIGE, multiple samples can be run and compared on the same gel without using spot matching programmes [7]. These 2D gel based MS methods offer high accuracy fold changes of proteins on the basis of the intensity of the protein spots on the gel. Unfortunately, these proteomics approaches provided only a very incomplete picture with some limitations for understanding of the molecular mechanisms underlying neuropathic pain at the protein level [14]. It has become apparent that 2D gels are almost exclusively restricted to cytosolic proteins and with a very low content of membrane proteins such as ion channels and receptors [9,

[10, 15]. Since many membrane proteins are of low abundance, enrichment of membranes or isolation of specific type of membrane proteins is beneficial for an extensive analysis. One of the approaches is the 1D gel based or gel-free MS strategies which are used to analyse integral membrane proteins [9]. These methods are not reliable for quantification on their own, therefore, additional methods for quantification have been developed. Isobaric tags such as iTRAQ have enabled quantitative analysis of samples without relying on 2D gels [16]. Recently more cost-effective methods, namely multiplex peptide stable isotope dimethyl labeling, have been developed [17]. Stable isotope dimethyl labeling does not require introduction of isotope labels at the organism level like SILAC (stable isotope labeling by amino acids in cell culture) [18, 19], and uses inexpensive reagents.

To capture the global protein changes in the CeA from the SNT model rats , we utilised three proteomics approaches in this work:- (a) the whole cell lysate of the CeA analysis using 2D-PAGE MS, (b) the purification of CeA membrane proteins and running them on the 1-SDS-PAGE, following by excising the gel band between 80 kDa to 230 kDa followed by the nano LC-MS/MS analysis of digested peptides, and (c) quantitative mass spectrometry-based proteomics analysis using triplex stable isotope dimethyl labeling of the CeA membrane proteins. We compared membrane proteomes of the CeA from Sham and rats at day 3, 7 and 21 after SNT surgery.

The 2D-gel based proteomic study revealed that more than 50 cytosolic proteins were altered in the CeA of SNT model rats. No significant proteome changes (F>4) was observed in the left- and right-side of the CeA. By using 1D-SDS-PAGE approach, we identified neurotransmitter receptors such as glutamate and GABA receptors, also sodium and potassium ion channel proteins, voltage-dependent ion channels such as potassium voltage-gated channel subfamily A member 3, Nav1.2. By using triplex stable isotope dimethyl labeling combined with the LC-MS/MS based proteomics, we identified more than 40 membrane proteins as differentially expressed proteins in the CeA of SNT model rats. These proteins may play roles in reciprocal relationship between pain and psychological distress in the amygdala and contribute to central sensitization. Doublecortin was identified with the highest fold change in all three biological replicates after the SNT surgery. Most of these changes of protein expressions were validated by qRT–PCR, western blotting and

immunochemistry.

Materials and Methods

Animals, SNT and sham surgery and Behaviour assessment

Two groups of animals were used in this study. The first group (Group 1) of animals were adult male Wistar rats (200 – 300 g) with spinal nerve transection (SNT model rats) produced by tight ligation and transection of the left L5 spinal nerve. Briefly, animals were anaesthetised using a mixture of medetomidine hydrochloride (0.25 mg/kg) and ketamine (60 mg/kg) administered in a single intra-peritoneal injection. The animals were placed in the prone position and under sterile conditions a paramedial incision was made to access the left L4-L6 spinal nerves. Approximately one-third of the L6 transverse process was removed. The L5 spinal nerve was identified and carefully dissected free from the adjacent L4 spinal nerve and then tightly ligated using 6-0 silk and then transected distally to the suture. The muscle layer was sutured, and the wound was closed with Vicryl 3-0. Mechanical withdrawal thresholds were tested using a Dynamic Plantar Aesthesiometer (Ugo Basile). A maximum cut-off of 50 g was used. The withdrawal threshold is calculated as the average of three consecutive tests with at least 10 min between each test. To measure cold hypersensitivity, we applied a drop of acetone to the plantar hindpaw and measured the time that the animal spent licking, shaking, or lifting the paw during the following 2 min. Sham rats underwent a skin incision, muscle dissection etc., but no injury was made in the spinal nerves. All behavioural tests were blinded to randomisation schedule. All animal experiments confirmed to the British Home Office regulations, and followed International Association for the Study of Pain guidelines for the care and use of animals. The animals were deeply anesthetised and decapitated, and their brains were frozen on dry ice within 3 min of decapitation and stored in -80ºC. Animals were culled on the days 3, 7 and 21 following surgery. Eight rats per each model were used for naïve, sham, SNT day 3, day 7 and day 21.

The second group (Group 2) were Wistar male rats initially weighing approximately 200 - 250 g. They underwent SNT surgery as described above. Animals were culled on days 7 and 14

following surgery, just after behavior study, and brains were immediately dissected and stored at -80ºC. Four rats per each model were used for naïve, SNT day 7 and day 14.

Dissection and location of the Central amygdale

The central amygdala (CeA) dissection was performed as follows:- The brain was placed on a black rubber stopper under a stereomicroscope and maintained at 4 ^{0}C, dorsal side up on. A coronal section was made at approximately bregma -1 and the second cut at approximately bregma -2.75 according Paxinos and Watson atlas with a razor blade. The thickness of the excised tissue was approximately 2,400 µm. The tissue was placed a cold stage caudal side up (nose down) and the central amygdala was micro-punched with a sample corer (1 mm ID x 3 mm OD) (Fine Science Tools). A total volume of the CeA is approximately 1.6 mm^3 and the wet weight of the punched samples (assuming that the density of the brain 1 mg/µL) would be around 1.5 mg, and a protein mass between 80 - 200 µg. The CeA tissues were stored at -80^{0}C.

To locate the area of central amygdala (CeA), brains from sham models were sectioned at 10 µm on a cryostat and stained with Nissl blue (Figure S1). Briefly, sections were defatted by immersing in a mixture of chloroform – methanol (1:1, vol/vol) for 1 hour, then washed in 100% ethanol, followed by 90% ethanol in water and 70% ethanol in water, after a short wash with water. The sections were immersed 0.1% cresyl violet acetate solution (Sigma) for 3 min, washed with water and dehydrated in 70% ethanol in water, 90% ethanol in water and 100% ethanol and coverslipped. Supplementary Information Figure S1 shows Nissl staining of the right-side of the rat brain slice, stereotaxic location at -1.8 relative to bregma.

Sample preparation for 2D-PAGE analysis

The CeA tissue was placed into 1.5-mL siliconised Eppendorf tubes containing 200 µL of hot (60°C) SDS sample buffer (2% w/v SDS in ultra-pure water) and sonicated using a Sonic Vibra Cell at amplitude 20% for 6 sec four times at 4ºC. Two per cent SDS solution is a good lysis buffer for brain tissues and readily penetrates cell membrane. After tissue lysates, the samples were heated to 60°C for 1 hour and centrifuged at 14,000 *xg* for 15 min at 4°C. The protein

concentration of the resulting supernatants was measured using BCA assay kit (Novagen) with BSA as the standard. Fifty µg of protein was loaded into a 500-µL Viva-spin concentrator column (GE Healthcare), diluted with the ultra-pure water to a 0.5% SDS concentration and centrifuged at 13,000 *xg* for less than 1 min to a final volume of 100 µL. Three hundred µL of an exchange buffer (8 M Urea, 2 M Thiourea and 2% CHAPS in water) was added to the sample. Note that the urea solution was deionised with an ion exchanger prior to adding the other chemicals, because urea in aqueous solution exists in equilibrium with ammonium cyanate which can react with the NH_3^+ of protein side chains (*e.g.* lysine) and introduce charge artifacts, leading to additional spots on the Isoelectric focusing (IEF) gel. The sample was centrifuged at 13,000 *xg* for 5 min to a final volume of 100 µL and this step was repeated 7 times. The final volume of each sample was around 100 µL. The protein concentration was measured using the RC DC Protein Assay Kit II with BSA standard (Bio-Rad Laboratories, UK). Just before isoelectric focusing to each protein sample was added DTT to a final concentration 20 mM and the samples were ultra-centrifuged at 40,000 *xg* for 20 min.

First-dimensional gel electrophoresis

Immobiline™ Dry Strip gels with a non-linear gradient pH 3-11NL were from GE Healthcare. We used eleven cm and twenty four cm Immobilized pH gradient (IPG) strips. The IPG strips were passively rehydrated overnight at room temperature to their original thickness of 0.5 mm with a solution containing DeStreak rehydration buffer (Amersham, UK) and 0.5% IPG buffer pH 3-11 (GE Healthcare), covered by a layer of silicone oil to prevent them from drying out. We found that DeStreak rehydration solution was more suitable for this protocol, as it prevented non-specific oxidation and streaking, also significantly improved reproducibility. After rehydration, the strips were transported to the Protean IEF focusing tray (Bio Rad). It is important to place electrode wicks in ultra-pure water after soaked on each IPG strip at the cathode and anode-ends. The electrode wicks served as receptacles for salt in the sample and improved the quality of the IEF step. A sample loading wells were placed at the anodic side of the IPG strips and were covered with mineral oil. Samples volumes of 40 - 100 µL were pipette into the sample loading wells.

Protein sample load was 60 µg per IPG strip. Isoelectric focusing was performed using Protean IEF cell system using the following program: 20 °C, 50 µA per strip; *step 1*, step-n-hold, 0.01 h, 50 V; *step 2*, step-n-hold, 4 h, 50 V; *step 3*, step-n-hold, 0.01 h, 500 V; *step 4*, step-n-hold, 4 h, 500 V; *step 5*, gradient, 4 h, for 11 cm pH 3-11NL IPG strips 6,000 V or for 24 cm pH 3-11NL IPG strips, 10,000 V; *step 6*, step-n-hold, 99 h, for 11 cm pH 3-11NL IPG strips 6,000 V or for 24 cm pH 3-11NL IPG strips, 10,000 V. The IEF for 11 cm IPG strips was performed to a total focusing time of 60,000 Vh; and for 24-cm IPG strips up to 100,000 Vh.

Second-dimension gel electrophoresis

Upon completion of IEF, the IPG strips were equilibrated to allow the separated proteins according to their *pI* values to fully interact with SDS. The IPG strips were incubated for 10-15 minutes in the equilibration buffer (50 mM Tris-HCl (pH 8.8), containing 2% (w/v) SDS, 1% (w/v) dithiothreitol (DTT), 6 M urea and 30% (w/v) glycerol). This is followed by a further 10-15 minute equilibration in the same solution containing 4% (w/v) iodoacetamide instead of DTT. The latter step was used to alkylate any free DTT, as otherwise it migrates through the second-dimension SDS-PAGE gel, resulting in an artifact known as point-streaking that can be observed after silver staining. More importantly, iodoacetamide alkylates sulfhydryl groups and prevents their re-oxidation. After equilibration, the IPG strips were washed in a gel electrophoresis running buffer then placed onto the surface of the SDS-PAGE gels, and covered with a layer of a 0.5% agarose in the running buffer with a pinch of bromophenol blue dye. For 24 cm IPG strips, the second dimension (SDS-PAGE) was performed in vertical 12% polyacrylamide gels using an Ettan DALT*six* System (Amersham) with the running buffer in the upper chamber and in the lower chamber, and ran at 20°C, 200 V until the bromophenol blue dye reached the 3/4 of gel boarder. The casting of four vertical SDS-PAGE gels (260 x 200 x 1.00 mm^3) were prepared from a mixture of 75 mL of 4x ProtoGel Resolving buffer (1.5M Tris-HCl, 0.4% SDS, pH 8.6, National Diagnostics), 90 mL of acrylamide-bis ready-to-use solution 40% (Merck RGaA), 135 mL of HPLC grade water, 300 µL of TEMED, and 3 mL of 10% APS solution. The mixture was filtered through a 0.2 µm filter (Sartorius Stedim Biotech, UK) and then poured into the caster gel DALTsix (VWR)

loaded with four glass plate DALT (260 x 200 x 1.00 mm^3). For 11 cm IPG strips, second dimension (SDS-PAGE) was carried out simultaneously on 4 slab polyacrylamide gels in a Bio Rad Protean II xi Cell system (Bio Rad) and ran at 50 V until the bromophenol blue dye migrated to the end of the stacking gels followed by 200 V till the dye migrated to the bottom of the gels, at 20 °C. The casting of four SDS-PAGE gels (125 x 65 x 1.0 mm^3) were prepared for a resolving buffer from a mixture of 36 mL acrylamide-bis ready-to-use solution 40% (Merck RGaA), 30 mL of 4x ProtoGel Resolving buffer (1.5M Tris-HCl, 0.4% SDS, pH 8.6, National Diagnostics, UK), 54 mL of HPLC grade water, 72 µL of TEMED, and 720 µL of 10% APS solution. A stacking buffer was prepared as follows:- 8 mL acrylamide-bis ready-to-use solution 40% (Merck RGaA), 8 mL of Stacking buffer (PAGE buffer solution pH 6.8, BDH, VWR), 30 mL of glycerol, 34 mL of HPLC grade water, 24 µL of TEMED, and 240 µL of 10% APS solution. All solutions were filtered before casting the gels as previously described. Gels were fixed in a fixing solution (45% ethanol, 45% water, 10% acetic acid) overnight and then stained using a silver staining mass spectrometry compatible kit (Thermo Fisher Scientific, UK) according to the manufacturer's instructions.

Image acquisition and Spot detection

Three biological replicates gels from each model, naïve, sham, SNT day 3, day 7, day 14 and day 21 were imaged using a Fujifilm Imager Reader LAS3000 immediately after the second dimension SDS-PAGE. The exposure time was optimised to achieve maximum dynamic range. Images were exported to TIFF format, and loaded for the spot detection using Progenesis SameSpots V 3.0 (Nonlinear Dynamics, UK). Gel images were aligned by automated calculation of alignment vectors after assigning manually thirty landmark vectors. Automatic analysis was performed on all aligned images using the analysis wizard. All the settings were left as defaults throughout the analysis. For protein identification by MS analysis a significance level of $p<0.1$ and spot area ≤ 50 were used to select spots to be excised from gel. The protein abundance of each spot in the images corresponding to the SNT and control samples was determined as a ratio compared with the intensity of the corresponding spot present in the known control image run in the same physical gel. Normalised volumes of the matched spots across all the gels were further

used to evaluate the statistical significance of differences between the SNT and control samples by Student's two-tailed t-test.

In-gel digestion of spots from 2D gels

The stained protein spots with fold change higher than 2 were excised from the gel, a control piece of gel also was cut from a blank region and processed in parallel with other spots. The gel pieces were destained according to the manufacture protocol (Thermo Fisher Scientific, UK), and washed with 200 µL ultra-pure water five times, followed by dehydration with 200 µL of 100% acetonitrile for 10 mins. Organic solvent was removed in a SpeedVac concentrator. Proteins were reduced with 10 mM dithiothreitol for 30 min at 37ºC, followed by alkylation with 55 mM iodoacetamide (IAA) for 60 min in the dark, and after washed with 25mM ammonium bicarbonate solution twice for 10 min. The gel pieces were dehydrated twice with 80% acetonitrile in 0.3% formic acid, and dried in the SpeedVac. To the dried gel pieces was added 20 µL of 12.5 ng/µL of trypsin (Promega, UK) in 25 mM ammonium bicarbonate and incubated overnight at 37ºC. The digestion was stopped by addition of formic acid to final concentration of 0.3%. For the MALDI-TOF/TOF-MS analysis, the supernatant was removed into a clean new Eppendorf vial and the gel pieces were incubated with 50 µL of 50% acetonitrile in 0.1% formic acid for 10 min, following by sonication for 20 min. The supernatant containing peptides were again collected into the same vial and the gel pieces were dehydrated with 50 µL of 100% acetonitrile for 10 min, followed by sonication for 20 min. The supernatants were pooled, organic solvent was removed in the SpeedVac to the final sample volume of around 10 µL. The peptide mixture was desalted on reversed phase C_{18} tips (Millipore) according to the manufacturer protocol, and the bound peptides were eluted in 1.5 µL of matrix (10 mg of α-cyano-4-hydroxycinnamic acid in 70% acetonitrile in 0.5% formic acid) and directly spotted onto the MALDI plate. For the nanoLC-MS/MS analysis, peptides were desalted on in-house manufactured reverse-phase tips, consisting of a plug of C_{18} matrix (3 m, Empore) packed into a 10-µL tip. Samples were acidified to 1% trifluoroacetic acid and tips pre-wetted and acidified with 100% methanol and 0.5% acetic acid, respectively, prior to application. Tips were washed with 0.5% acetic acid and peptides

eluted with 0.1% trifluoroacetic acid in 75% acetonitrile and lyophilised in a vacuum concentrator. Lyophilised peptides were re-suspended in 3 µL of 0.5% acetonitrile in 0.1% TFA and analysed by nanoLC-ES-MS/MS.

MALDI-TOF/TOF-MS analysis of 2D-PAGE of the excised spots

MS/MS measurement was carried out on a 4700 Proteomics-Analyser (Applied Biosystems). The spectra recorded in reflector mode in a mass range from 700 to 4000 Da with a focus mass of 2000 Da. If the autolytic fragment trypsin with the monoisotopic $[M+H]^+$ *m/z* at 842.510 or 2211.104 reached S/N of at least 10, an internal calibration was automatically performed using this peak for one-point-calibration. The internal calibration was automatically performed as one-point-calibration if the monoisotopic arginine $[M+H]^+$ *m/z* at 175.119 or lysine $[M+H]^+$ *m/z* at 147.107 reached S/N of at least 5. The MALDI-MS resolution for the peptides was ~10,000, and the mass accuracy was 10 – 20 ppm. The MS/MS resolution was 3,000 - 6,000. After calibration, a combined database search of MS and MS/MS measurements was performed using the GPS Explorer software (Applied Biosystems, UK) with the following settings:- (a) MS peak filtering: mass range from 700 to 4000 Da; minimum S/N filter of 10, mass exclusion list contained background peaks and trypsin fragments with an exclusion tolerance of 100 ppm; (b) MS/MS peak filtering: mass range from 60 Da to a mass that was 20 Da lower than the precursor mass; (c) database search: precursor tolerance 35 ppm and MS/MS fragment tolerance 0.3 Da. Peak lists were compared with the Swiss-Prot or NCBInr database restricted to rattus taxonomy using the MASCOT search engine (Matrix Science). Peptide mixtures that yielded at least twice a MOWSE score[2] of at least 50 for Swiss-Prot and 63 for NCBInr results, respectively, were defined as positive identifications.

Identification of high molecular weight membrane proteins by using 1D-SDS-PAGE gel

One-dimensional SDS-PAGE was performed using standard methods on the Hoefer Mighty Small gel system (Amersham). Membrane protein samples were prepared as described below only the final membrane pellet was reconstituted in 2% SDS, 50 mM Tris-HCl, pH 6.8. Membrane protein

samples were heated at 50° C for 10 min in a solubilisation buffer (2% SDS, 20% glycerol, 0.01% bromophenol blue, and 50 mM Tris-HCl, pH 6.8) and 0.1 M dithiothreitol. Membrane protein (5 µg) was resolved on a self-made 10% acrylamide gel. Gels were placed in a fixing solution (45% ethanol, 45% water, 10% acetic acid) overnight and then stained using a silver staining mass spectrometry compatible kit (Thermo Fisher Scientific, UK) according to the manufacturer's instructions.

In-Gel Tryptic Digestion and Peptide Extraction

The molecular weight region on the SDS-PAGE gel between 230 and 80 kDa was divided into five approximately equal bands, and each band was excised with a scalpel. Bands were washed in distilled water and destained according to the manufacturer's protocol. Bands were cut into fine pieces to increase the surface area, dried with acetonitrile, and then in a SpeedVac (Thermo Savant) for 5 min. Digestion was carried out using sequencing-grade modified trypsin (approximately 75 ng/µL) (Promega, UK) in 25 mM NH_4HCO_3. Sufficient trypsin solution was added to swell the gel pieces, which were kept on ice for 30 min and then covered with 25 mM NH_4HCO_3 and incubated at 37° C overnight. Peptides were extracted from the gel pieces with ultrasonication, using sequential washings with a solution of 5% formic acid (FA) in 50% acetonitrile and 70% methanol in 0.1% FA. The extracts were combined and dried in a SpeedVac to dryness and reconstituted in 5 µL 0.2% FA, following C18 desalting (Empore Octadecyl C18, Sigma), the samples were analysed by nanoLC-MS/MS.

Nano LC-ES-MS/MS analysis of the excised spots from 2D-PAGE and tryptic digested peptides from 1D-SDS-PAGE gel excised between gel regions 80 kDa to 230 kDa

The LC-MS/MS system consisted of an LTQ Orbitrap XL or an LTQ Orbitrap Velos (Thermo Fisher Scientific) equipped with an ESI probe coupled to a Dionex Ultimate 3000 HPLC system (Dionex,UK) fitted with a nanospray ion source (Proxeon, UK). The samples were injected through a 10-µL loop in a pick-up injection mode, 1 µL per sample. The injected peptides were separated on a C18 analytical column, which was prepared by packing a Picotip spray emitter (150 mm length, 100 µm internal diameter, New Objective) with ProntoSIL C18 phase matrix

(120-Å pore size, 3-µm bead size, Bischoff Chromatography). Peptides separated using two different gradient programs with a mobile phase A of 0.1% formic acid in water, and mobile phase B of 0.1% formic acid in 80% acetonitrile. The first one provides a separation of the majority of peptides and requires a shorter time, and was used for peptides extracted from spots of 2D-gels. The second longer gradient was developed in order to provide a more separation of peptides and increase a chance to detect low abundance peptides and more hydrophobic peptides derived from the 1D-gel band of membrane proteins. The shorter LC gradient was as follows. After 3 min with 2% B, the mobile phase composition was raised to 5% B and was raised again to 20% over 12 min, and then to 50% B over the next 15 min, and then raised sharply over 0.2 min to 90% B, maintained at 90% B for a further 5 min, before returning to 2% B to recondition the column at 2% B for 5 min. The total gradient time was 40 min. The flow rate was 300 nL/min, and the eluent was directed to the ESI source of the LTQ-Orbitrap mass spectrometer. The second gradient was used for the identification of membrane proteins and was as follows. After 3.1 min at 2% B, the proportion of B was raised to 15% B over the next 32 min using gradient curve 8 (Chromeleon software, Dionex, UK). The proportion of B was then increased to 60% over 75 min, before returning to 20% B in 0.1 min. The column was re-equilibrated for a 10 min giving a total run time of 120 min. The flow rate was 300 nL/min, and the eluent was directed to the ESI source of the LTQ-Orbitrap mass spectrometer. MS data was acquired using a data-dependent acquisition mode, and operated at 60,000 resolution (full width at half maximum height, FWHM definition), and the top five 2+, 3+ and 4+ ions in the 300 - 1800 *m/z* were selected for MS/MS. Charge state 1+ ions were rejected. The automatic gain control for the Orbitrap was set to 500,000 ions, and the automatic gain control for the MS/MS in the ion trap was set at 10,000 ions. For MS/MS the isolation width was set at 2, the collision energy was 35%. Three MS/MS microscans for each precursor were accumulated. Maximum injection time into the ion trap in MS/MS was 200 ms, and maximum accumulation time in the Orbitrap was 500 ms. Dynamic exclusion was enabled, and selected ions were excluded for 180 s before they could be selected for another round of MS/MS.

Protein identification

MS/MS peak lists were converted to mzXML format using ReAdW version 4.4.1 (LTQ XL Orbitrap data). This tool was used with default parameters except that zlib compression of spectral data was enabled. Data was uploaded to the central proteomics facilities pipeline (CPFP at: https://cpfp-master.molbiol.ox.ac.uk/cpfp_demo/auth/login) or https://mascot.molbiol.ox.ac.uk (www.proteomics.ox.ac.uk). Files were searched using Mascot version 2.3.01 (Matrix science), X!TANDEM version 2008.12.01.1 and OMSSA version 2.1.8 against a concatenated target and reversed decoy version of the IPI rat sequence database (EBI), versions 3.79 containing 78,946 target protein sequences and 41,806,600 residues. Enzyme was set to trypsin (or chymotrypsin for some experiments) allowing for up to 3 missed cleavages. Carbamidomethyl (C) was set as a fixed modification, and acetyl (N-term), deamidated (NQ), oxidation (M) were set as variable modifications. Mass tolerances for MS and MS/MS peak identifications were 20 ppm and 0.6 Da respectively. The level of confidence for peptide identifications was based on the Mascot assignment of "identity" ($p<0.05$). Protein identifications were only made when two or peptides from that protein were identified with Mascot scores above the identity threshold. In cases where the identified protein was a member of a multiprotein family with similar sequences, the protein identified was the one with the highest number of matched peptide identification rate.

Classification of differentially expressed proteins identified by 2D-PAGE MS

Database searches were carried out using BLAST algorithm at the National Center for Biotechnology Information (NCBI), and the ProteinCenter version 3.3 (http://thermo.proteincenter.proxeon.com/ProXweb/app) and KEGG database (www.genome.jp/kegg) was used to obtain general information concerning the biological function of the differentially expressed proteins from gel- and MS-based proteomics. The Gene Ontology (GO) annotations of proteins were compared with the ones from a reference proteome (e.g., identified proteins vs the entire protein database or a subset of the identified proteins vs the overall identified proteins).

Membrane protein purification by the differential centrifugation

The CeA tissues were placed into an ice-cold glass homogeniser, along with approximately 1 mL of homogenisation buffer for every 0.1 g of tissue, and sonicated using the Sonic Vibra Cell at amplitude 20% for 6 sec four times at 4ºC. The homogenisation buffer contained 0.25 M sucrose, 50 mM TEAB, pH 7.4 at 4^0C, protease inhibitor cocktail (Sigma-Aldrich, USA). All solutions were prepared in ultra-pure water (Fluka, UK). After sonication, the samples were left on ice for 1 hour. Membrane fractions were prepared using differential centrifugation as follows:- an initial centrifugation at 10,000 *xg* for 10 min at 4ºC was used to sediment the cell debris, nuclei and unbroken cells. The supernatant was centrifuged at 100,000 *xg* for 30 min at 4ºC. The pellets from this step were re-suspended in 100 mM sodium carbonate (Sigma-Aldrich, USA) and left for 30 min on ice. Samples were then centrifuged at 100,000 *xg* for 30 min at 4ºC. The resultant pellets were washed three times with ultra-pure water and then re-suspended in 40 µL of 0.2% Protease MAX™ Surfactant (Promega, UK) in 50 mM TEAB. The samples were mixed by vortexing for 2 minutes at medium speed. Proteins were found to become soluble within 40 minutes. All samples were stored at -80ºC. The membrane protein concentrations were determined using the BCA assay kit.

In-solution digestion of membrane proteins

Five µg of protein of each sample was taken for an on-column stable isotope dimethyl labelling and put into new Eppendorf tubes. The samples volume was adjusted to 93.5 µL with 50 mM TEAB and 1 µL of 0.5 M DTT was added. The samples were then incubated at 56 ^{0}C for 20 min, followed by addition of 2.7 µL of 0.55 M iodoacetamide and incubated at room temperature in the dark for 15 min. After 1 µL of 1% Protease MAX™ Surfactant and 1.8 µL of 1 µg/µL Trypsin Gold (Promega) were added to the samples and left overnight at 37^0C in a water bath. The samples were centrifuged at 12,000 xg for 10 seconds and digestion was stopped by addition of 5 µL of formic acid (Merck). Note: Protease MAX™ Surfactant is a hydrophobic anionic surfactant (sodium-3((1-(furan-2-yl)undecyloxy)carbonylamino)propane-1-sulfonate) and degrade over the course of a digestion reaction. However, for a complete degradation of the surfactant the samples

were incubated for 10 min at 37 ^{0}C. The concentration of peptides was determined by UV-spectrometry using an extinction coefficient of 1.1 for 0.1% (g/L) solution at 280 nm.

On-column triplex stable isotope dimethyl labelling of the membrane proteins

Stable isotope dimethyl triplex labelling at the peptide level was performed as described by Boersema et al. [17]. Equal amounts of protein were labelled on-column using “light”, “medium” and “heavy” dimethyl labelling reagents and the three channels were mixed in a 1:1:1 ratios. In brief, 5 µg of tryptic digested proteins per channel in 50 mM TEAB, 5% formic acid were applied on an individual home-made µC18 Stage Tips. The µC18 Stage Tips were made as described by Neugebauer et al. [3]. Briefly, a 10-µL tips were blocked with a 3 mg of Sep-Pak Classic C18 stationary phase (Waters) was sandwiched with another layer of and the adapter with 1-mL syringe was used as a pressure device. The µC18 tips were pre-washed three times with 450 µL of acetonitrile, followed by three washes with 0.6% (vol/vol) acetic acid in water. This followed by loading each of the three samples on a separate µC18 tip. The µC18 Stage tips were washed with 450 µL of 0.6% (vol/vol) acetic acid in water followed by application of 225 µL of respective stable isotope dimethyl labelling solution (“light”, “intermediate” or “heavy”). The on-column labelling solutions were prepared per sample/label. Four hundred fifty µL of 50 mM sodium phosphate buffer, pH 7.5 was mixed with 25 µL of 4% (vol/vol) formaldehyde in ultra-pure water (CH_2O (37% (vol/vol), cat no. 25,254-9, Sigma), CD_2O (20%, 98% D, Isotec) or $^{13}CD_2O$ (20%, 99% ^{13}C, 96% D, Sigma-Aldrich, USA) and 25 µL of 0.6 M cyanoborohydride in ultra-pure water (sodium cyanoborohydride or sodium cyanoborodeuteride, 96% D). The resulting eluent were re-applied ten times on the same µC18 Stage tips to allow complete labelling and this took at least 30 min. After the µC18 Stage tips were washed with 450 µL of 0.6% (vol/vol) acetic acid in water. The labelled peptides were eluted from the µC18 Stage tips with 150 µL of 0.6% (vol/vol) acetic acid in 80% acetonitrile. The differently labelled samples were mixed and dried in a SpeedVac to 10 µL, then acidified to 0.25% with formic acid and immediately analysed by nanoLC-MS/MS.

Nano LC-MS/MS analysis of triplex stable isotope dimethyl labelled peptides and data analysis

The LC-MS/MS system consisted of a Q Exactive mass spectrometer (Thermo Fisher Scientific, UK) equipped with a nano ESI probe coupled to an Ultimate 3000 RSLCnano system (Dionex, UK). Chromatographic separation was performed using a a NanoEASY (Thermo Fisher Scientific) C_{18} reverse-phase column (50 cm long, 75 µm internal diameter, 2 µm beads) at a flow rate of 300 nL min^{-1}. Mobile phase A consisted of 0.1% formic acid in 5% acetonitrile. Mobile phase B consisted of 0.1% formic acid in 80% acetonitrile. A 290 min gradient was used to separate the dimethyl labelled peptides and each sample was typically injected three times and data merged in order to increase sample coverage and a LC gradient method was as follows:- After 20 min at 5% B, the proportion of B was raised to 30% B over the next 180 min (using gradient curve 8 Chromeleon software, Dionex, UK). The proportion of B was then increased to 50% over 60 min, and further increased to 98% over the next 10 min before returning to 5% B in 0.1 min. The column was re-equilibrated for a 10 min. The eluent was directed to the ESI source of the Q Exactive mass spectrometer. The mass spectrometer was operated in a 'top 10' data-dependent acquisition mode with dynamic exclusion enabled (40 s). Survey scans (mass range 300 - 1,650 Th) were acquired at a resolution of 70,000 at 200 Th with the ten most abundant multiply charged ($z \geq 2$) ions selected with a 3-Th isolation window for fragmentation by higher-energy collisional dissociation. MS/MS scans were acquired at a resolution of 17,500 at 200 Th.

Protein identification and quantification

Quantification of peptide triplets was processed using Proteome Discoverer 1.3, version 1.3.0.339 (Thermo Fisher Scientific). MS/MS peak lists were converted to mgf format using ProteoWizard msconvert release 3.0.3535 (Q Exactive data). Searches against the UniProt rat database [20, 21] were performed using Mascot (version 2.3.01). Mascot was set up in its special quantification mode in which the N-terminal and lysine demethylation was set as an interconnected modification (i.e. when the peptide is dimethyl labelled on a lysine residue, the N terminus is also expected to be labelled with the same isotopomeric dihyl label and vice versa) to lower the number of false-positive identifications of peptides with different isotope labels. We treated three technical nano-LC-MS/MS runs as replicates and combined them during software analysis generating one .msf

file corresponding to one biological replicate. Two biological replicates were used. Trypsin was chosen as cleavage specificity allowing two missed trypsin cleavage sites, maximum modification per peptide 4. Search parameters were precursor mass tolerance 10 ppm, fragment mass tolerance 0.1 Da. Carbamidomethylation (C) set as a static modification. Dynamic modifications were oxidation (M), dimethyl (K), dimethyl (N-term), dimethyl-4 (K), dimethyl-4 (N-term), dimethyl-8 (K) and dimethyl-8 (N-term). The peptide validator node was set to "false". The "RT tolerance of isotope pattern multiplets" parameter was set to 0.3 min. We required proteins to have a minimum of two quantifiable unique peptides. Proteome Discoverer Peptide results were filtered to 1% false discovery rate, peptides length 6 - 35, peptide score >20%, maximum search engine rank 1 and peptide mass deviation 7 ppm. For reporting the quantitation data we set fold change higher than 2 and FDR ≥ 0.5%. Proteins that were not reproducibly quantified across biological replicates were removed from downstream analysis. Then, all the quantification results were normalised against the log2 of the median ratio of all the quantified peptides and reported as the log2 Day3 (or Day 7) or Day 21 to Sham.

Western Blot

Fifteen µg of protein of the CeA tissue lysates (these samples were prepared as described in *sample preparation for 2D-PAGE analysis section*) and the membrane protein (samples were prepared as described in *membrane protein extraction section)* samples (sham; n=3, naïve; n=3, SNT day 3, 7 and 21; n=3) in 100 mM Tris-HCl, pH 6.8, 30% glycerol, 2% SDS, 0.0025% bromophenol blue, 100 mM DTT were heated at 60^0C for 20 min and then were loaded on 10% poly-acrylamide/bis-acrylamide TRIS-HCl discontinuous gels. Proteins were transferred onto polyvinylidene fluoride (PVDF) membrane (GE Healthcare) using the iBlot DRY Blotting system for 15 min at 20 V (Invitrogen, UK). Membranes were washed three times in TBS, 0.1% Triton X-100 (TBS-T) each time 10 min, and then blocked in 5% BSA, TBS-T for 1 hour at RT, subsequently washed three times for 5 min in TBS-T. Afterwards, the membranes were incubated with anti-DCX (1:700, ab23542, Abcam) in 5% BSA, TBS-T for 1 h at RT. Following three washes, the membranes were incubated with the secondary goat anti-rabbit HRP antibody

(1:1000, Dako) in 5% BSA, TBS-T for 1 h at RT. The PVDF membranes were then washed three times with TBS-T, bands were visualised using a chemiluminescence kit (AppliChem, UK) and detection with the Fujifilm LAS-3000 Imaging System. Ponceau staining was used as control for equal protein load and transfer.

Immunohistochemistry

To study the co-localisation of Doublecortin (DCX) with cell compartment markers, a triplex-labelling immunohistochemistry technique was used. We used three representative animals each form SNT day 7 and day 21 rats. After embedding the dissected brain tissue as described above in OCT compound (Sakura Finetek), 10-µm-thick coronal sections were cut on a cryostat, mounted on poly-L-lysine-coated glass slides, and air-dried for 3 hours at room temperature. The 1st and 3rd sections were mounted on positively coated glass slides three sections per slide. Five slides per animal were selected per brain region for each immunostaining. The brain sections were rinsed three times for 10 min in PBS and then post-fixed in 4% paraformaldehyde in phosphate buffer for 15 minute, followed by again three times wash in phosphate buffer. Afterwards, sections were incubated in blocking solution (PBS, pH 7.4, 0.3% Triton X-100, 2 mg/mL BSA, 5% normal goat serum for 60 min at RT. Primary antibodies were diluted in fresh blocking solution and applied overnight at 4ºC. The primary antibodies used were as follows:- anti-α1 Na,K-ATPase (1:200, mouse monoclonal; ab7671), anti-58K Golgi protein (1:200, mouse monoclonal; ab27043), anti-Doublecortin (1:100, rabbit polyclonal; ab23542) from Abcam. Next, the brain sections were washed in PBS for 30 min at room temperature and subsequently incubated for 2 hours in the dark with the appropriate fluorescent secondary antibody (anti-mouse or anti-rabbit IgG conjugated with FITC - Red or TRITC - Green, Dako, UK) diluted 1:200 in blocking solution. Following three additional rinses in PBS, sections were finally cover slipped using Vectashield water-based mounting medium with DAPI (Vector Laboratories). The analysis of negative controls (omission of primary antibody) was simultaneously performed in order to exclude the presence of non-specific immunofluorescent staining, cross-immunostaining, or fluorescence bleed-through. Samples were analysed on a wide-field Nikon 80i microscope and

pictures acquired with an ultrahigh-quality Nikon DXM1200F digital camera controlled with LUCIA G software.

Quantitative real-time PCR Analysis

For quantitative RT-PCR, RNA from sham and SNT day 3, day 7, day 14 and day 21 CeA tissues were extracted using a peqGOLD MicroSpin Total RNA kit (Qiagen, UK). One ng of each RNA sample was used per analysis. The RNA was then reverse transcribed using the SuperScript III First-Strand Synthesis System kit (Invitrogen). Real time PCR was performed using the StepOnePlus System and the 2x Fast SYBR Green Master Mix (Applied Biosystems), to accurately determine target gene expression levels. PCR reactions were performed in a total reaction volume of 20 µL, containing 10 µL SYBR Master Mix, 8 µL of 0.125 ng/µL cDNA for each model and 2 µL of both forward and reverse primers (10 µM each). Samples were loaded in triplicate on the plate for each primer set, and both GAPDH and γWHAZ were used as housekeeping genes. The PCR was run with an initial step of 95 °C for 20 seconds to activate the AmpliTaq Fast DNA polymerase enzyme, followed by 40 cycles of 95 °C for 3 seconds, 59 °C (annealing) for 15 seconds and 72 °C for 15 seconds. Fluorescence incorporation of the SYBR Green to double stranded DNA was measured after each cycle, to generate an amplification curve. Product composition was verified at the end of each reaction with melt curve analysis in 0.6 °C increments from 60 °C to 95 °C. Primer sequences (5' to 3'), with annealing temperatures of 60 °C and amplicon size < 250 bp.

Results

Identification of differentially expressed proteins in neuropathic pain models by 2D-gel

The objective of this work was to identify the proteins with altered expression levels in the central amygdala of neuropathic pain animals. Identifying these proteins would be valuable for understanding the mechanism of neuropathic pain. We first studied protein expression profiles in the protein extract from rats after and before SNT surgery using 2D-gels. The silver-stained

protein spots were quantitatively analysed and protein spots with a fold-change higher than or equal to 2 and $p < 0.1$ were considered as a significant change in this work. Protein spots were excised from 2D-gels, subjected to *in-gel* trypsin digestion and peptides were analysed by peptide mass fingerprinting using a MALDI-TOF/TOF mass spectrometer (MALDI-TOF/TOF-MS) or alternatively by nano-LC-MS/MS analyses. We performed preliminary studies by capillary-LC-ES-MS/MS using the LCQ mass spectrometer to evaluate the protein identification from silver-stained 2D-gels prior to more detail studies on the Orbitrap instruments. Nano-LC-MS/MS runs, we performed on a nano-LC connected to either of two mass spectrometers Orbitrap XL or Orbitrap Velos. Two groups of neuropathic pain rat models were used in this study. For each neuropathic pain model, we generated 2D-gels of three biological replicates and three technical replicates. We compared protein changes in the right and left CeA of naïve versus rats at 7 and 14 days after SNT surgery (group 1), whereas, sham or naive versus rats at days 3, 7 and 21 after SNT surgery represents group 2. The behavioural results on the animals used in this research were as reported in previous studies [22-24]. The behavioural data on the animals used in this research have been published previously

We used an 11 cm long IPG strips with pH 3-11 for group 1. Both the naïve group and SNT group gels detected around 1,600 spots per each gel (after exclusion of false spots). Figure 1 shows a representative 2D-gel. We performed gel-to-gel matching of spots with the reference gel, defined to be the gel containing the most spots and non-matching spots were removed after careful and rigours manual validation. We matched around 1,500 spots in the CeA gels. Tables 1 to 5 summarise the differentially expressed proteins. Briefly, we identified the same proteins for these spots by above two nano-LC-MS/MS systems. It should be taken into consideration that as a maximum of 3,000 spots can be observed on a typical 2D-gel by silver staining, many proteins will inevitably co-migrate to the same spot position, thus confounding their accurate quantitation and mass spectrometric identification, and also some of these proteins maybe expressed in different quantities in CeA. We found that the products of two genes migrated to the same faint spot on a silver-stained. However, the identity of protein was taken with the highest MASCOT

score, although maybe low-abundance proteins are a true fold-change. There is lateralisation of pain processing in the amygdala [18, 19, 25, 26]. Higher neuronal activity in the right than in the left CeA after formalin administration and in a model of arthritic pain was previously reported [25, 27].

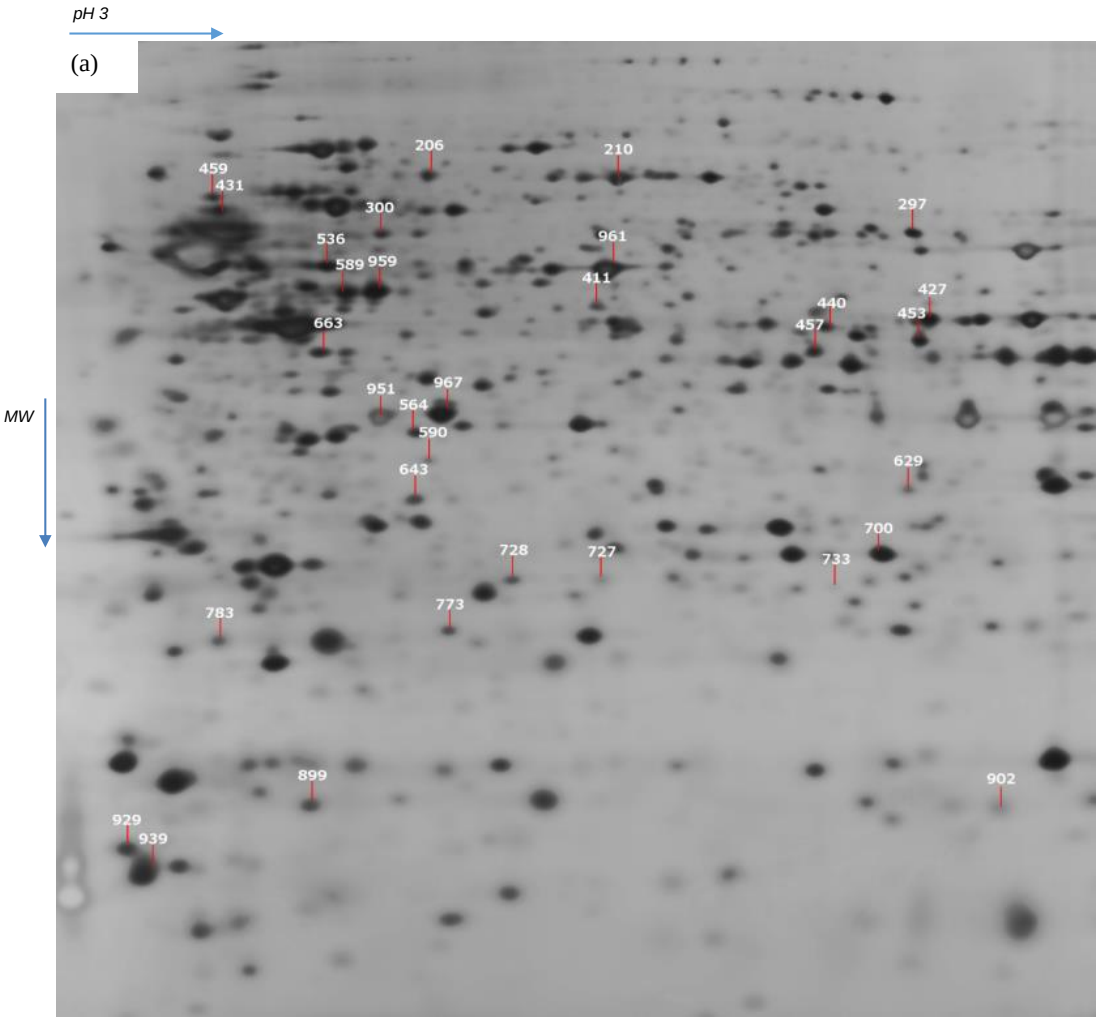

Figure 1 Silver stained 2D-gel of (a) the right-side CeA and (b) the left-side CeA. Thirty three spots were differentially detected with F≥2 as shown by arrows. Using Progensis SameSpot software was utilised for the cross-comparison analysis between 2D-gels of naïve and rats at day 7 and 14 post SNT surgery. The first dimension, an isoelectric focusing (IEF), was pefomed with an immobilised pH gel (pH 3-11NL) of 11 cm long, where proteins separated according to *pI* values. The second dimension, SDS-PAGE was perfomed, with a 12% SDS polyacrylamide gel, where the proteins are separated by their molecualr weight.

TABLE 1. Indentified proteins by nanoLC-MS/MS from spots excised from 2D-gels, 11 cm IPG strip corresponding to the 1st group of neuropathic pain rat models. The central amygdala was excised from the Left- and Right-sides of rat brain. 2D-gels of the Left- and Right-sides of CeA were compared using Protein Progenesis Software, protein spots with a fold-change higher than or equal to 2 and $p < 0.1$ were excised and proteins extracted and digetsed with trypsin followed by nanoLC-MS/MS analysis on the Orbitrap Velos Pro mass spectrometer

Spots	Accession no (SwissProt)	Protein description	Mascot score	MW	*pI*	Seq. Cov. (%)	Fold change comparison between Right- and Left-sides of CeA in Native, SNTs day 7 and day 14, **2<F>3**
297	P15999	ATP synthase subunit alpha, mitochondrial	865	59831	9.22	38.2	right -side of SNT day 7
297	Q5XI77	Anxa11 RCG39189, isoform CRA_a	821	54468	7.53	38.6	
297	Q6P6V0	Glucose-6-phosphate isomerase	457	62958	7.38	22.2	
429	P16617	Phosphoglycerate kinase 1	702	44909	8.02	53.0	right -side of SNT day 7
429	Q8VHF5	Citrate synthase, mitochondrial	494	52176	8.53	29.4	
429	P05065	Fructose-bisphosphate aldolase A	173	39783	8.31	25.3	
429	P15999	ATP synthase subunit alpha, mitochondrial	124	59831	9.22	23.0	
429	Q9JJ54	Heterogeneous nuclear ribonucleoprotein D0	94	38339	7.62	17.0	
429	P17764	Acetyl-CoA acetyltransferase, mitochondrial	92	45009	8.92	14.9	
783	Q6P7Q4	Lactoylglutathione lyase	224	20977	5.12	36.4	right -side of SNT day 7
783	P28073	Proteasome subunit beta type-6	205	25502	4.85	16.8	
783	O35509	Ras-related protein Rab-11B	160	24588	5.64	27.1	
902	P10111	Peptidyl-prolyl cis-trans isomerase A	124	18091	8.34	31.7	right-side of Naïve
948	P15999	ATP synthase subunit alpha, mitochondrial	2814	59831	9.22	67.3	right-side of Naïve and SNT day 14
948	Q6AXS5	Plasminogen activator inhibitor 1 RNA-binding protein	94	44841	8.6	19.0	
948	Q8R4T5	General receptor for phosphoinositides 1-associated scaffold protein	39	42637	9.16	17.0	
951	P54313	Guanine nucleotide-binding protein G(I)/G(S)/G(T) subunit beta-2	564	38048	5.6	33.5	right-side of Naïve
951	P42123	L-lactate dehydrogenase B chain	254	36874	5.7	27.5	
951	P81799	N-acetyl-D-glucosamine kinase	213	37458	5.55	11.7	

Therefore, we examined if there are protein changes between the right and the left of CeA in naïve and SNT models (Supporting Information, Figure S2). From these matched spots with the *t* test and 2-fold change as cut off we found one spot 948 was significantly different between the left- and right-CeA in naïve and SNT model rat at day 14, and was identified as a mitochondrial protein - metabolic enzyme, specifically ATP-synthase subunit α, which produces ATP from ADP in the presence of a proton gradient across the membrane. Four spots were increased with fold change between 2<F>3 in the right-side of CeA after SNT surgery at day 7 (Table 1). Spot 297 was identified as Annexin A11, which has complex and essential functions in several biological pathways including apoptosis and proliferation. Spot 429 was identified as phosphoglycerate kinase 1. Phosphoglycerate kinase is a transferase enzyme used in the seventh step of glycolysis, thus deficiency of this kinase is a genetic disorder that affects the body's ability to break down the simple sugar glucose. We found four significantly increased spots in the right-side of CeA versus the left- after SNT surgery at day 14. Spot 902 was identified as peptidyl-prolyl *cis*-trans isomerase A, which accelerates the folding of proteins. We identified seven proteins with MASCOT score higher than 50 for spot 951 of the 2D-gel most likely due to posttranslational modification and co-migration of similar molecular weight and *pI* values proteins. Several guanine

nucleotide-binding proteins (G proteins) were identified with a highest MASCOT score for this spot.

We then compared 2D-gels of the right CeA from naïve versus SNT rats. Thirty three matched spots showed significant differences and twenty six of them were identified by nano-LC-MS/MS and by peptide finger printing using MALDI-TOF/TOF analyses (Figure 1). These instruments were used to further verify the identity of proteins, so the proteins which were identified by two instruments were considered as a true fold-change. According to Progenesis Same Spot analysis of 2D-gels, sixteen spots were down-regulated in the right CeA after SNT at day 14. Twenty two protein spots were down-regulated in the right CeA between day 7 and 14 after SNT surgery. One protein spot was up-regulated between day 7 and day 14 after SNT surgery and two protein spots were up-regulated at day 7 after SNT surgery. A summary of the identified proteins is presented in Table 2. For example, spot 961 was identified as calcium/calmodulin dependent protein kinase type II subunit α. This protein is a prominent kinase in the central nervous system (CNS) that may function in long-term potentiation and neurotransmitter release. Spot 939 was identified as enoyl-CoA hydrase, which has neurotrophic and neuroprotective properties on a broad spectrum of CNS neurons and it promotes cell survival. Spot 590 was identified as Annexin 3 encodes a protein that exhibits calcium-dependent phospholipid binding. Spot 411 was identified as mitogen-activated protein (MAP) kinases, which are serine/threonine-specific protein kinases that respond to extracellular stimuli and modulates cellular activities, such as proliferation, cell survival and apoptosis. Spot 728 was identified as perodoxin-6, which belong to antioxidant enzymes and plays a role in the regulation of phospholipid turnover as well as in protection against oxidative injury. Spot 959 was identified as creatine kinase B. This protein was previously reported as down-regulated after nerve injury [7, 20, 21, 28, 29], this is in an agreement with our study. The highest fold-change of 4.62 was detected for spot 961 between day 7 and day 14 after SNT surgery.

TABLE 2. Indentified proteins by nanoLC-MS/MS from spots excised of 2D-gels, 11 cm IPG strip corresponding to the 1st group of neuropathic pain rat models. The central amygdala was excised from the Left-side of rat brain

	Spot No	Accession no (SwissProt)	Protein description	Mascot score	MW	*pI*	Seq. Cov. (%)	Fold change Left-CeA	Identified by
1	128	Q9ER34	Aconitate hydratase, mitochondrial precursor	450	85,433	5.80	45	↑ (2.5)	nanoLC-LTQ Orbirtap XL
2	233	Q9QUL6	Vesicle-fusing ATPase	356	82,652	6.55	20	↑ (2.4)	nanoLC-LTQ Orbirtap XL
3	337		n/d					↓(2.5)	nanoLC-LTQ Orbirtap XL
4	459	P07335	Creatine kinase B-type	117	42,725	5.42	52	↑ (2.9)	nanoLC-LTQ Orbirtap XL
	459	P82995	Heat shock protein HSP 90-alpha	95	84,815	5.01	39	↑ (2.9)	nanoLC-LTQ Orbirtap XL
	459	F1LTA7	Uncharacterized protein (Fragment)	69	42,385	5.21	28	↑ (2.9)	nanoLC-LTQ Orbirtap XL
	459	D4A2Z9	Uncharacterized protein	54	80,700	4.91	31	↑ (2.9)	nanoLC-LTQ Orbirtap XL
	459	F1M5B6	Uncharacterized protein (Fragment)	42	76,900	5.34	22	↑ (2.9)	nanoLC-LTQ Orbirtap XL
	459	D4AE04	Uncharacterized protein	39	57,300	5.22	25	↑ (2.9)	nanoLC-LTQ Orbirtap XL
	459	D3ZE66	Uncharacterized protein	31	64,700	5.12	34	↑ (2.9)	nanoLC-LTQ Orbirtap XL
5	472	P11980	Pyruvate kinase isozymes M1/M2	234	57,819	6.63	21	↓ (2.9)	nanoLC-LTQ Orbirtap XL
6	510		n/d					↓ (2.6)	nanoLC-LTQ Orbirtap XL
7	519		n/d					↓ (2.5)	nanoLC-LTQ Orbirtap XL
8	534	Q5XI34	Protein phosphatase 2 (Formerly 2A)	804	65,323	4.75	35	↓ (2.9)	nanoLC-LTQ Orbirtap XL
	534	Q4QQT4	Serine/threonine-protein phosphatase 2A 65 kDa regulatory subunit A beta	789	66,006	4.73	23	↓ (2.9)	nanoLC-LTQ Orbirtap XL
	534	Q6P9V9	Tubulin alpha-1B chain	403	50,152		25	↓ (2.9)	nanoLC-LTQ Orbirtap XL
	534	P50398	Guanosine diphosphate dissociation inhibitor 1, isoform CRA_a	345	50,538	4.75	9	↓ (2.9)	nanoLC-LTQ Orbirtap XL
	534	P34058	Heat shock protein HSP 90-beta	201	83,281	5.03	49	↓ (2.9)	nanoLC-LTQ Orbirtap XL
9	548		n/d					↑ (2.3)	nanoLC-LTQ Orbirtap XL
10	552	O54937	Pyruvate dehydrogenase kinase isoform 4	32	46,679	6.47	26	↓ (2.7)	nanoLC-LTQ Orbirtap XL
11	578		n/d						nanoLC-LTQ Orbirtap XL
12	602	P60203	Myelin proteolipid protein	70	30,077	8.71	19	↓ (2.6)	nanoLC-LTQ Orbirtap XL
13	614	G3V6D3	ATP synthase subunit beta	656	56,345	5.27	77	↑ (2.7)	nanoLC-Orbitrap Velos Pro MS
	614	P69897	Tubulin beta-5 chain	220	49,671	4.89	54	↑ (2.7)	nanoLC-Orbitrap Velos Pro MS
	614	P06761	78 kDa glucose-regulated protein	131	72,347	5.16	58	↑ (2.7)	nanoLC-Orbitrap Velos Pro MS
	614	P07323	Gamma-enolase	70	47,141	5.16	45	↑ (2.7)	nanoLC-Orbitrap Velos Pro MS
14	624	P42123	L-lactate dehydrogenase B chain	253	36,612	5.92	37	↓ (2.5)	nanoLC-LTQ Orbirtap XL
15	638	Q497B0	Omega-amidase NIT2	241	30,701	6.90	15	↓ (3.4)	nanoLC-LTQ Orbirtap XL
16	658		n/d					↓ (3.6)	nanoLC-LTQ Orbirtap XL
17	674	P48500	Triosephosphate isomerase	929	26,849	7.29	45	↓ (2.6)	nanoLC-LTQ Orbirtap XL
18	702	Q3T1K5	F-actin-capping protein subunit alpha-2	512	32,967	5.65	30	↓ (1.9)	nanoLC-LTQ Orbirtap XL
	702	P42123	L-lactate dehydrogenase B chain	160	36,612	5.92	27	↓ (1.9)	nanoLC-LTQ Orbirtap XL
19	728	O35244	Peroxiredoxin-6	501	24,819	5.64	29	↓ (1.5)	nanoLC-LTQ Orbirtap XL
20	730	P22062	Protein-L-isoaspartate(D-aspartate) O-methyltransferase	142	24,641	7.14	20	↓ (2.0)	nanoLC-LTQ Orbirtap XL
21	740	P09527	Ras-related protein Rab-7a	365	23,504	6.40	48	↑ (2.7)	nanoLC-LTQ Orbirtap XL
	740	Q6NYB7	Ras-related protein Rab-1A	292	22,678	5.93	41	↑ (2.7)	nanoLC-LTQ Orbirtap XL
	740	P61589	Transforming protein RhoA	283	21,782	5.83	40	↑ (2.7)	nanoLC-LTQ Orbirtap XL
	740	P10536	Ras-related protein Rab-1B	262	22,163	5.55	37	↑ (2.7)	nanoLC-LTQ Orbirtap XL
	740	O35509	Ras-related protein Rab-11B	223	24,489	5.64	18	↑ (2.7)	nanoLC-LTQ Orbirtap XL
	740	Q4KM73	UMP-CMP kinase	196	22,169	5.66	26	n/d	nanoLC-LTQ Orbirtap XL
22	755	Q5U316	Ras-related protein Rab-35	94	23,025	8.52	17	↑(2.5)	nanoLC-LTQ Orbirtap XL
	755	P97576	GrpE protein homolog 1, mitochondrial	43	24,297	8.57	15	↑(2.5)	nanoLC-LTQ Orbirtap XL
23	772	P39069	Adenylate kinase isoenzyme 1	249	21,584	7.66	28	↓ (2.5)	nanoLC-LTQ Orbirtap XL
24	797	P37805	Transgelin-3	90	22,501	7.44	24	↓ (3.0)	nanoLC-LTQ Orbirtap XL
25	874	Q6LED0	Histone H3.1	30	15,404	11.71	34	↑(2.5)	nanoLC-LTQ Orbirtap XL
	874	P62804	Histone H4	93	11,367	11.90	27	↑(2.5)	nanoLC-LTQ Orbirtap XL
	874	P0C0S7	Histone H2A.Z	58	13,422	11.29	25	↑(2.5)	nanoLC-LTQ Orbirtap XL
26	883	O88767	Protein DJ-1	152	19,974	6.77	24	↑(2.6)	nanoLC-LTQ Orbirtap XL
	883	P19804	Nucleoside diphosphate kinase	200	17,283		28	↑(2.6)	nanoLC-LTQ Orbirtap XL
27	899	P63025	Vesicle-associated membrane protein 3	100	11,480	7.85	31	↓ (2.0)	nanoLC-LTQ Orbirtap XL
	899	Q63228	Glia maturation factor beta	89	16,736	5.32	41	↓ (2.0)	nanoLC-LTQ Orbirtap XL

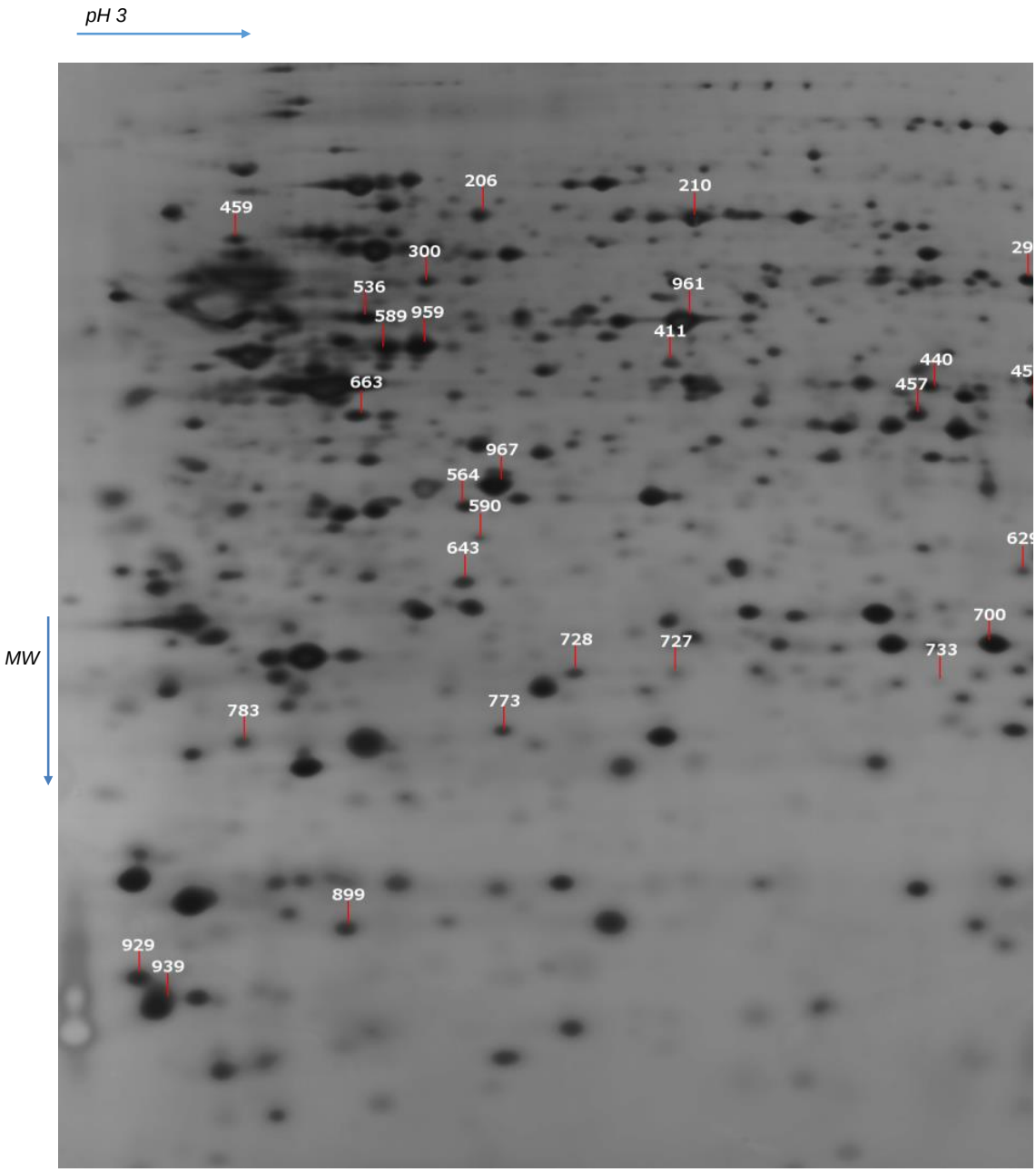

Figure 2. 2D-gel of the left-side CeA. Arrows indicate spots with fold change ≥ 2, when 2D-gels of naïve compared to 2D-gels of neuropathic pain model rats at day 7 and 14 post SNT surgery.

TABLE 3. Indentified proteins by nanoLC-MS/MS from spots excised from 2D-gels, 11 cm IPG strip corresponding to the 1st group of neuropathic pain rat models. The central amygdala was excised from the Right-side of rat brain

No	Spot No	Accession no (SwissProt)	Protein description	Mascot score	MW	*pI*	Seq. Cov. (%)	Fold change Right-CeA	Identified by
1	206	Q6P3V7	Tetratricopeptide repeat protein GNN	29	150,287	8.89	16	↓ (2.0)	nanoLC-Orbitrap Velos Pro MS
		Q99JD4	CLIP-associating protein 2	35	141,463	8.79	15	↓ (2.0)	nanoLC-Orbitrap Velos Pro MS
2	210	P23348	Anion exchange protein 3	35	135,407	6.06	15	↓ (2.1)	nanoLC-Orbitrap Velos Pro MS
3	297	P15999	ATP synthase subunit alpha, mitochondrial	865	59,754	9.22	38	↓ (2.0)	nanoLC-LTQ Orbitap XL
		Q5XI77	Annexin A11	821	54,160	7.77	39	↓ (2.0)	nanoLC-LTQ Orbitap XL
		Q6P6V0	Glucose-6-phosphate isomerase	457	62,827	7.89	22	↓ (2.0)	nanoLC-LTQ Orbitap XL
4	300		n/d					↓ (2.0)	nanoLC-LTQ Orbitap XL
5	411	P85515	Alpha-centractin	171	42,614	6.19	43	↓ (3.2)	nanoLC-LTQ Orbitap XL
		Q01986	Dual specificity mitogen-activated protein kinase kinase 1	163	43,465	6.18	27	↓ (3.2)	nanoLC-LTQ Orbitap XL
6	427		n/d					↑(2.0)	
7	431	P50398	Rab GDP dissociation inhibitor alpha	1461	51,074	5.00	69	↑(2.9)	nanoLC-LTQ Orbitap XL
		Q9Z0W5	Protein kinase C and casein kinase substrate in neurons protein 1	102	50,760	5.15	25	↑(2.9)	nanoLC-LTQ Orbitap XL
8	440		n/d					↑(2.1)	nanoLC-LTQ Orbitap XL
9	453	Q2LAM0	Fatty acid 2-hydroxylase	29	42,673	7.1	28	↓ (2.0)	nanoLC-LTQ Orbitap XL
10	457	O54937	Pyruvate dehydrogenase kinase isoform 4	32	46,679	6.5	46	↓ (2.0)	nanoLC-LTQ Orbitap XL
11	459	P07335	Creatine kinase B-type	117	42,725	5.42	52	↑(2.9)	nanoLC-LTQ Orbitap XL
		P82995	Heat shock protein HSP 90-alpha	95	84,815	5.01	39	↑(2.9)	nanoLC-LTQ Orbitap XL
		F1LTA7	Uncharacterized protein (Fragment)	69	42,385	5.21	28	↑(2.9)	nanoLC-LTQ Orbitap XL
		D4A2Z9	Uncharacterized protein	54	80,700	4.91	31	↑(2.9)	nanoLC-LTQ Orbitap XL
		F1M5B6	Uncharacterized protein (Fragment)	42	76,900	5.34	22	↑(2.9)	nanoLC-LTQ Orbitap XL
		D4AE04	Uncharacterized protein	39	57,300	5.22	25	↑(2.9)	nanoLC-LTQ Orbitap XL
		D3ZE66	Uncharacterized protein	31	64,700	5.12	19	↑(2.9)	nanoLC-LTQ Orbitap XL
12	536	P23565	Alpha-internexin	197	56,115	5.22	64	↑(2.1)	nanoLC-LTQ Orbitap XL
		P63039	60 kDa Heat shock protein, mitochondrial	149	60,955	6.18	44	↑(2.1)	nanoLC-LTQ Orbitap XL
		P63018	Heat shock cognate 71 kDa protein	77	70,871	5.52	46	↑(2.1)	nanoLC-LTQ Orbitap XL
		P61980	Heterogeneous nuclear ribonucleoprotein K	62	50,976	5.54	35	↑(2.1)	nanoLC-LTQ Orbitap XL
13	564		n/d					↑(2.7)	nanoLC-LTQ Orbitap XL
14	589	P34058	Heat shock protein HSP 90-beta	201	83,281	5.03	49	↑(3.0)	nanoLC-LTQ Orbitap XL
		P82995	Heat shock protein HSP 90-alpha	170	84,815	5.01	38	↑(3.0)	nanoLC-LTQ Orbitap XL
		E9PSZ3	Spectrin alpha chain, non-erythocytic 1	48	284,900	5.38	15	↑(3.0)	nanoLC-LTQ Orbitap XL
15	590	P14669	Annexin A3	172	36,363	5.96	13	↓ (2.9)	nanoLC-LTQ Orbitap XL
		P20759	Ig gamma-1 chain C region	39	36,493	6.43	19	↓ (3.2)	nanoLC-LTQ Orbitap XL
16	629	Q9Z2L0	Voltage-dependent anion-selective channel protein 1	168	30,756	8.62	48	↓ (3.5)	nanoLC-LTQ Orbitap XL
	629	Q6PCU2	V-type proton ATPase subunit E 1	130	26,128	8.44	35	↓ (3.5)	nanoLC-LTQ Orbitap XL
17	643	P32851	Syntaxin-1A	57	33,067	4.9	13	↓ (2.5)	nanoLC-LTQ Orbitap XL
18	663	F1LTA7	Uncharacterized protein (Fragment)	74	42,385	5.67	5	↓ (3.0)	nanoLC-LTQ Orbitap XL
19	700	P48500	Triosephosphate isomerase	1575	26,849	7.29	38	↓ (2.1)	nanoLC-LTQ Orbitap XL
20	727	P63012	Ras-related protein Rab-3A	146	24970	4.9	22	↑(2.1)	nanoLC-LTQ Orbitap XL
		Q63942	GTP-binding protein Rab-3D	146	24290	4.8	18	↑(2.1)	nanoLC-LTQ Orbitap XL
21	728	O35244	Peroxiredoxin-6	501	24,819	5.64	25	↓ (2.0)	nanoLC-LTQ Orbitap XL
22	733		n/d					↑(2.1)	nanoLC-LTQ Orbitap XL
23	773	P04906	Glutathione S-transferase P	101	23,439	7.44	12	↓ (2.0)	nanoLC-LTQ Orbitap XL
		P48500	Triosephosphate isomerase	35	26,849	7.29	19	↓ (2.0)	nanoLC-LTQ Orbitap XL
24	783	Q6P7Q4	Lactoylglutathione lyase	236	20,820	5.12	33	↓ (3.3)	nanoLC-LTQ Orbitap XL
		P28073	Proteasome subunit beta type-6	154	25,290	4.85	28	↓ (3.3)	nanoLC-LTQ Orbitap XL
		O35509	Ras-related protein Rab-11B	134	24,489	5.65	21	↓ (3.3)	nanoLC-LTQ Orbitap XL
		Q5XI73	Rho GDP-dissociation inhibitor	128	23,450	5.12	29	↓ (3.3)	nanoLC-LTQ Orbitap XL
		Q00981	Ubiquitin carboxyl-terminl hydrolase isozyme L1	120	25,165	5.14	22	↓ (3.3)	nanoLC-LTQ Orbitap XL
25	899	P63025	Vesicle-associated membrane protein 3	100	11,480	7.85	31	↓ (2.6)	nanoLC-LTQ Orbitap XL
		Q63228	Glia maturation factor beta	89	16,736	5.32	41	↓ (2.6)	nanoLC-LTQ Orbitap XL
26	902	P10111	Peptidyl-prolyl cis-trans isomerase A	124	17,874	8.33	32	↓ (2.4)	nanoLC-LTQ Orbitap XL
		Q9Z1B2	Glutathione S-transferase Mu 5	67	26,629	6.74	15	↓ (2.4)	nanoLC-LTQ Orbitap XL
27	929	Q63754	Beta-synuclein	135	14,495	4.48	19	↓ (2.3)	nanoLC-LTQ Orbitap XL
		Q6PEC4	S-phase kinase-associated protein 1	70	18,831	4.4	20	↓ (2.4)	nanoLC-LTQ Orbitap XL
28	939		n/d					↓ (2.5)	nanoLC-LTQ Orbitap XL
29	940	P25113	Phosphoglycerate mutase 1	478	28,832	6.67	17	↓ (2.6)	nanoLC-LTQ Orbitap XL
		P14604	Enoyl-CoA hydratase, mitochondrial	377	31,516	8.39	29	↓ (2.6)	nanoLC-LTQ Orbitap XL
30	951	P54313	Guanine nucleotide-binding protein G(I)/G(S)/G(T) subunit beta-2	564	37,331	5.85	34	↑(2.8)	nanoLC-LTQ Orbitap XL
		P42123	L-lactate dehydrogenase B chain	254	36,612	5.92	28	↑(2.8)	nanoLC-LTQ Orbitap XL
		P81799	N-acetyl-D-glucosamine kinase	213	37,196	5.76	12	↑(2.8)	nanoLC-LTQ Orbitap XL
31	959	P07335	Creatine kinase B-type	362	42,725	5.39	27	↓ (2.6)	nanoLC-LTQ Orbitap XL
		Q9JKB7	Guanine deaminase, isoform CRA_b	221	50,901	5.56	35	↓ (2.6)	nanoLC-LTQ Orbitap XL
32	961	P04764	Alpha-enolase	1147	47,127	6.53	23	↓ (4.6)	nanoLC-LTQ Orbitap XL
		P11275	Calcium/calmodulin-dependent protein kinase type II subunit	506	54,088	6.61	32	↓ (4.6)	nanoLC-LTQ Orbitap XL
		P11730	Calcium/calmodulin-dependent protein kinase type II subunit gamr	28	59,685	7.63	18	↓ (4.6)	nanoLC-LTQ Orbitap XL
		P07323	Gamma-enolase	243	47,141	4.91	54	↓ (4.6)	nanoLC-LTQ Orbitap XL
		Q1KYT0	Beta-enolase	575	47,130		34	↓ (4.6)	nanoLC-LTQ Orbitap XL
33	967		n/d					↓ (2.2)	

We also investigated the protein fold-changes in the left CeA of naïve rats versus the left CeA of rats at day 7 and day 14 after SNT surgery (Figure 2), summarised in Table 3. Twenty two matched spots showed significant difference, and eighteen spots produced positive identification of proteins. We identified more than two proteins in eighteen spots of the 2D-gel by using nano-LC-MS/MS and peptide finger printing MALDI-TO2/TOF analyses, but identity of the proteins with the highest MASCOT score are discussed below. The highest fold-change (spot 638) was 3.69 between day 7 and day 14 after SNT surgery, and was identified as omega-amidase NIT 2. The role of this protein is to remove potentially toxic intermediates. Spot 131 was produced the identity of N-ethylmaleimide-sensitive fusion protein and was down-regulated in SNT models at day 7, but up-regulated in SNT models at day 14. This protein is essential for numerous calcium triggered vesicle trafficking events. This protein functions as a molecular chaperone. It was previously reported that interaction between N-ethylmaleimide-sensitive factor and glutamate receptor is essential for fear memory formation in CeA [20, 21, 30]. Spot 730 presented the identity of L-isoaspartyl methyltransferase (PIMT), this protein catalyses repair of L-isoaspartyl peptide bonds, a major source of protein damage. It was previously reported that PIMT knock-out mice exhibit brain enlargement and fatal epileptic seizures [6, 7, 20, 21]). Spot 772 was identified adenylate kinase, along with creatine kinase. Spot 899 was identified as vesicle-associated membrane proteins (VAMPs) encodes a protein that exhibits SNARE binding (soluble N-ethylmaleimide sensitive factor attached protein receptor), and was previously reported to up-regulated during nerve regeneration [31].

Gene expression analysis of significantly changed fourteen proteins in the right-side of CeA and nineteen proteins in the left-side of CeA was performed by quantitative real-time PCR to further access the regulation at the transcriptional level (Figures 3). The 2-fold change of these proteins occurred in rats between day 7 and day 14 after SNT surgery. Comparison of fourteen transcript changes with the proteomics data (Figure 3a) revealed that all fourteen changes in the same direction (thirteen lower and one higher expression in SNT model rats), whereas only one protein

showed opposite mRNA expression compared to protein expression in the left-side CeA (Figure 3b, NSF).

(a)

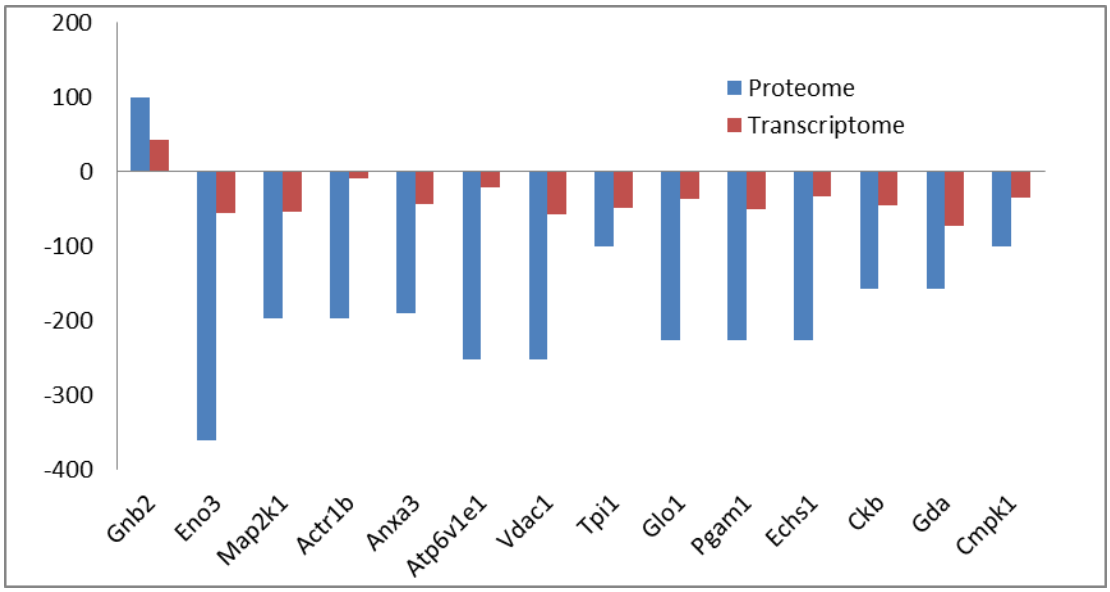

(b)

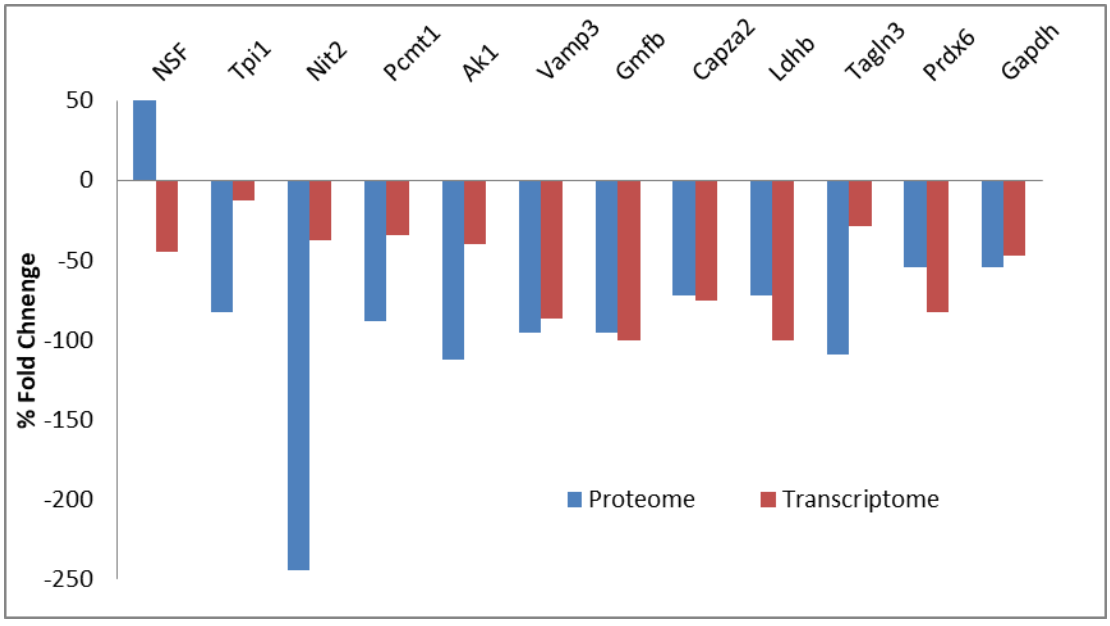

Figure 3. Transcriptome versus Proteome (a) the right-side of CeA (b) the left-side of CeA for Group 1.

The protein expression profiles from the right- and left- side of CeA from sham and rats at day 3, 7 and 21 after SNT surgery were compared (Group 2). The proteins were resolved on a 24 cm long IPG strip pH 3-11 and we loaded around 30 µg of protein per gel. Using this IPG strip approximately 2,100 spots were detectable per gel by silver staining. Two representative 2D-gels for the left- and the right-sides of CeA as compared between sham versus day 3, 7 and 21 after SNT surgery were shown in Figures 4 and 5. Through differential analysis with Progenesis SameSpot software, and comparison of the average spot intensity changes in the left-side of CeA of sham versus rats at 3, 7 and 14 days after SNT surgery we detected eighteen spots as significantly regulated with a fold-change ≥ 2. These spots were excised and proteins from fifteen spots were successfully identified by mass spectrometry. Each identified protein is listed Tables 4 and 5, linked to the corresponding 2D-gel spot in Figures 4 and 5. Ten spots were consistently of decreasing intensity, two spots generated changes between day 7 and day 21 after SNT surgery and one spot between day 3 and day 7. Spot 459 was identified as Rab GDP dissociated inhibitor α and protein kinase C and casein kinase substrate in neurons protein 1. The identities of these proteins were confirmed by nano-LC-MS/MS analysis and MALDI-TOF/TOF analysis. These proteins were also up-regulated in group 1 on the left-side of CeA. Protein kinase C and casein kinase substrate in neurons protein 1 may play a role in vesicle formation and transport [1, 5-7, 20, 21, 32]. Spot 1599 gave a multiple identity of proteins and these proteins were up-regulated in SNT models, and also detected in group 1 as up-regulated proteins (Tables 1, 2).

TABLE 4. Indentified proteins by nanoLC-MS/MS from spots excised from 2D-gels, 24 cm IPG strip corresponding to the 2nd group of neuropathic pain rat models. The central amygdala was excised from the Left-side of rat brain

No	Spots	Fold	Up/Down-regulated	Accession no (SwissProt)	Protein description	Mascot score	MW	*pI*	Seq. Cov. (%)	Instrumentation
1	374	2.4	↓	P47942	Dihydropyrimidinase-related protein 2	823	62,278	6.33	14	nanoLC-LTQ Orbirtap XL
			↓	Q62950	Dihydropyrimidinase-related protein 1	673	62,499	6.64	44	nanoLC-LTQ Orbirtap XL
			↓	Q62951	Dihydropyrimidinase-related protein 4	234	61,617	6.3	34	nanoLC-LTQ Orbirtap XL
2	428	2.7	↓(D21); ↑(D3,D7)	P11980	Pyruvate kinase isozymes M1/M2	456	58,294	6.63	20	nanoLC-LTQ Orbirtap XL
			↓(D21); ↑(D3,D7)	Q4KM49	Tyrosyl-tRNA synthetase, cytoplasmic	286	59,420	6.57	20	nanoLC-LTQ Orbirtap XL
			↓(D21); ↑(D3,D7)	Q62952	Dihydropyrimidinase-related protein 3	243	62,327	6.04	11	nanoLC-LTQ Orbirtap XL
			↓(D21); ↑(D3,D7)	P19332	Microtubule-associated protein tau	68	78,801	5.95	19	nanoLC-LTQ Orbirtap XL
3	459	2.9	↑	P07335	Creatine kinase B-type	117	42,725	5.42	52	nanoLC-Orbitrap Velos Pro MS
			↑	P82995	Heat shock protein HSP 90-alpha	95	84,815	5.01	39	nanoLC-Orbitrap Velos Pro MS
			↑	F1LTA7	Uncharacterized protein (Fragment)	69	42,385	5.21	28	nanoLC-Orbitrap Velos Pro MS
			↑	D4A2Z9	Uncharacterized protein	54	80,700	4.91	31	nanoLC-Orbitrap Velos Pro MS
			↑	F1M5B6	Uncharacterized protein (Fragment)	42	76,900	5.34	22	nanoLC-Orbitrap Velos Pro MS
			↑	D4AE04	Uncharacterized protein	39	57,300	5.22	25	nanoLC-Orbitrap Velos Pro MS
			↑	D3ZE66	Uncharacterized protein	31	64,700	5.12	19	nanoLC-Orbitrap Velos Pro MS
4	498	2.5	↑	Q63537	Synapsin-2	471	63,702	8.70	25	nanoLC-LTQ Orbirtap XL
			↑	B2GV06	Succinyl-CoA:3-ketoacid-coenzyme A transferase 1, mitochondrial	384	56,624	8.70	30	nanoLC-LTQ Orbirtap XL
			↑	Q6P6R2	Dihydrolipoyl dehydrogenase, mitochondrial	305	54,574	7.96	18	nanoLC-LTQ Orbirtap XL
5	599	2.5	↑	P50554	4-aminobutyrate aminotransferase, mitochondrial	269	57,161	8.15	28	nanoLC-LTQ Orbirtap XL
6	630	2.3	↓	Q9QXQ0	Alpha-actinin-4	419	42,052	5.27	26	nanoLC-LTQ Orbirtap XL
			↓	P04764	Alpha-enolase	417	47,440	6.16	47	nanoLC-LTQ Orbirtap XL
			↓	P63269	Actin, gamma-enteric smooth muscle	278	42,249	5.31	36	nanoLC-LTQ Orbirtap XL
			↓	P18298	S-adenosylmethionine synthase isoform type-2	166	44,030	5.93	13	nanoLC-LTQ Orbirtap XL
			↓	Q6AYZ1	Tubulin alpha-1C chain	112	50,590	4.96	12	nanoLC-LTQ Orbirtap XL
			↓	Q3MIE4	Synaptic vesicle membrane protein VAT-1 homolog	110	43,319	6.17	28	nanoLC-LTQ Orbirtap XL
			↓	Q68FR6	Elongation factor 1-gamma	108	50,371	6.31	17	nanoLC-LTQ Orbirtap XL
			↓	Q3KRE8	Tubulin beta-2B chain	104	50,377	4.78	19	nanoLC-LTQ Orbirtap XL
			↓	P62909	40S ribosomal protein S3	99	26,828	9.68	31	nanoLC-LTQ Orbirtap XL
7	679	2.8	↓	Q01986	Dual specificity mitogen-activated protein kinase kinase 1	1208	43,779	6.18	50	nanoLC-LTQ Orbirtap XL
			↓	P07936	Neuromodulin	102	23,703	4.61	20	nanoLC-LTQ Orbirtap XL
8	773	2.9	↓	Q5M7U6	Actin-related protein 2	267	44,990	6.30	42.4	nanoLC-LTQ Orbirtap XL
			↓	F1LPS8	Transcriptional activator protein Pur-alpha	116	34,976	6.07	17.4	nanoLC-LTQ Orbirtap XL
9	810	3.1	↑(D3,D7)		n/d					nanoLC-LTQ Orbirtap XL
10	933	2.5	↑		n/d					nanoLC-LTQ Orbirtap XL
11	993	4.0	↓	Q498U4	SAP domain-containing ribonucleoprotein	200	23,647	6.30	23	nanoLC-LTQ Orbirtap XL
12	1024	2.2	↓	B2RYW9	Fumarylacetoacetate hydrolase domain-containing protein 2	488	34,958	8.63	43	nanoLC-LTQ Orbirtap XL
13	1184	3.1	↑(D3); ↓(D7,D21)	Q6P0K8	Junction plakoglobin	121	82,490	5.75	23	nanoLC-LTQ Orbirtap XL
			↑(D3); ↓(D7,D21)	P60711	Actin, cytoplasmic 1	107	42,052	5.29	41	nanoLC-LTQ Orbirtap XL
			↑(D3); ↓(D7,D21)	F1LMV6	Protein Dsp (Desmoplakin)	88	334,582	6.45	15	nanoLC-LTQ Orbirtap XL
14	1338	2.9	↓	Q642A5	DNA polymerase epsilon subunit 3	33	16,674	4.39		MALDI-TOF/TOF
15	1342	2.0	↓	P04916	Retinol-binding protein 4		23,220	5.77	49	MALDI-TOF/TOF
16	1374	2.6	↓	P07632	Cu/Zn superoxide dismutase [Rattus norvegicus]		15,912	6.34	21	nanoLC-LTQ Orbirtap XL
			↓	P37805	Transgelin-3	27	22,500	7.44		MALDI-TOF/TOF
17	1503	2.2	↓	P31044	Phosphatidylethanolamine-binding protein 1	538	20,902	5.48	75	nanoLC-LTQ Orbirtap XL
18	1591	2.5	↑	P22062	Protein-L-isoaspartate(D-aspartate) O-methyltransferase	120	24,683	7.14	45	MALDI-TOF/TOF
19	1599	2.6	↑	P50398	Rab GDP dissociation inhibitor alpha	1461	51,074	5.00	69	nanoLC-LTQ Orbirtap XL
		2.6	↑	Q9Z0W5	Protein kinase C and casein kinase substrate in neurons protein 1	102	50,760	5.15	25	nanoLC-LTQ Orbirtap XL
			↑	Q5XI34	Protein Ppp2r1a	195	65,323	5.11	53	nanoLC-Orbitrap Velos Pro MS
			↑	P24090	Alpha-2-HS-glycoprotein, isoform CRA_b		38,002			nanoLC-LTQ Orbirtap XL
20	1664	2	↑	P11980	Isoform M2 of Pyruvate kinase isozymes M1/M2	330	58,294	6.63	45	nanoLC-LTQ Orbirtap XL
		2	↑	P12928	Pyruvate kinase isozymes R/L	64	62,504	6.45	19	nanoLC-LTQ Orbirtap XL
		2	↑	P62630	Elongation factor 1-alpha 1	63	50,424	9.10	13	nanoLC-LTQ Orbirtap XL
		2.0	↑	O88758	Potassium voltage-gated channel subfamily S member 1		54,914	7.66	45	MALDI-TOF/TOF
21	1724	2.4	↑		n/d					nanoLC-LTQ Orbirtap XL

TABLE 5. Indentified proteins by nanoLC-MS/MS from spots excised from 2D-gels, 24 cm IPG strip corresponding to the 2nd group of neuropathic pain rat models. The central amygdala was excised from the Right -side of rat brain

Spots	Fold	Up/Down-regulated		Accession no	Protein description	Mascot score	MW	*pI*	Seq. Cov. (%)	Instrumentation
459	2.5	↑	KCRB_RAT	P07335	Creatine kinase B-type	117	42,725	5.42	52	nanoLC-LTQ Orbitrap XL
		↑	HS90A_RAT	P82995	Heat shock protein HSP 90-alpha	95	84,815	5.01	39	nanoLC-LTQ Orbitrap XL
		↑	F1LTA7_RAT	F1LTA7	Uncharacterized protein (Fragment)	69	42,385	5.21	28	nanoLC-LTQ Orbitrap XL
		↑	D4A2Z9_RAT	D4A2Z9	Uncharacterized protein	54	80,700	4.91	31	nanoLC-LTQ Orbitrap XL
		↑	F1M5B6_RAT	F1M5B6	Uncharacterized protein (Fragment)	42	76,900	5.34	22	nanoLC-LTQ Orbitrap XL
		↑	D4AE04_RAT	D4AE04	Uncharacterized protein	39	57,300	5.22	25	nanoLC-LTQ Orbitrap XL
		↑	D3ZE66_RAT	D3ZE66	Uncharacterized protein	31	64,700	5.12	19	nanoLC-LTQ Orbitrap XL
507	3.1	↑	PDIA3_RAT	P11598	Protein disulfide-isomerase A3	360	57,044	5.88	31	nanoLC-LTQ Orbitrap XL
		↑	PRS4_RAT	P62193	26S protease regulatory subunit 4	101	49,325	5.87	40	nanoLC-LTQ Orbitrap XL
		↑	SEPT9_RAT	Q9QZR6	Septin-9	80	65,169	7.14	25	nanoLC-LTQ Orbitrap XL
		↑	PRS4_RAT	P62193	26S protease regulatory subunit 4	111	49,325	5.87	29	nanoLC-Orbitrap Velos Pro MS
		↑	ACTB_RAT	P60711	Actin, cytoplasmic 1	109	42,052	5.29	40	nanoLC-Orbitrap Velos Pro MS
		↑	DC1L1_RAT	Q9QXU8	Cytoplasmic dynein 1 light intermediate chain 1	100	56,985	6.13	11	nanoLC-Orbitrap Velos Pro MS
510	2.4	↑	G6PI_RAT	Q6P6V0	Glucose-6-phosphate isomerase	595	62,958	7.38	37	nanoLC-LTQ Orbitrap XL
		↑	SYN2_RAT	Q63537	Synapsin-2	323	63,702	8.73	25	nanoLC-LTQ Orbitrap XL
		↑	CAP1_RAT	Q08163	Adenylyl cyclase-associated protein 1	173	51,899	7.16	12	nanoLC-LTQ Orbitrap XL
		↑	SCOT1_RAT	B2GV06	Succinyl-CoA:3-ketoacid-coenzyme A transferase 1, mitochondrial	112	56,624	8.70	9	nanoLC-LTQ Orbitrap XL
534	2.8	↑	Q5XI34_RAT	Q5XI34	Protein phosphatase 2 (Formerly 2A)	401	65,323	4.75	25	nanoLC-LTQ Orbitrap XL
		↑	2AAB_RAT	Q4QQT4	Serine/threonine-protein phosphatase 2A 65 kDa regulatory subunit A beta	367	66,006	4.73	35	nanoLC-LTQ Orbitrap XL
		↑	TBA1B_RAT	Q6P9V9	Tubulin alpha-1B chain	230	50,152		43	nanoLC-LTQ Orbitrap XL
		↑	GDIA_RAT	P50398	Guanosine diphosphate dissociation inhibitor 1, isoform CRA_a	127	50,538	4.75	23	nanoLC-LTQ Orbitrap XL
614	2.0	↑	ATPB_RAT	P10719	ATP syntase subunit beta, mitochondrial	120.0	56,354	4.92	18	MALDI-TOF/TOF
		↑	SNP29_RAT	Q9Z2P6	Synaptosomal-associated protein 29	51.0	29,071	5.12	17	MALDI-TOF/TOF
		↑	G3V6D3_RAT	G3V6D3	ATP synthase subunit beta	656.21	56,345	5.27	77	nanoLC-Orbitrap Velos Pro MS
		↑	TBB5_RAT	P69897	Tubulin beta-5 chain	219.82	49,671	4.89	54	nanoLC-Orbitrap Velos Pro MS
		↑	G3V7C6_RAT	G3V7C6	Protein Tubb2c	218.9	49,831	4.89	48	nanoLC-Orbitrap Velos Pro MS
		↑	ENOG_RAT	P07323	Gamma-enolase	69.57	47,141	5.16	45	nanoLC-Orbitrap Velos Pro MS
		↑	GRP78_RAT	P06761	78 kDa glucose-regulated protein	130.54	72,347	5.16	58	nanoLC-Orbitrap Velos Pro MS
630	2.6	↓	ACTN4_RAT	Q9QXQ0	Alpha-actinin-4	419	42,052	5.27	26	nanoLC-LTQ Orbitrap XL
		↓	ENOA_RAT	P04764	Alpha-enolase	417	47,440	6.16	47	nanoLC-LTQ Orbitrap XL
		↓	ACTH_RAT	P63269	Actin, gamma-enteric smooth muscle	278	42,249	5.31	36	nanoLC-LTQ Orbitrap XL
		↓	METK2_RAT	P18298	S-adenosylmethionine synthase isoform type-2	166	44,030	5.93	13	nanoLC-LTQ Orbitrap XL
		↓	TBA1C_RAT	Q6AYZ1	Tubulin alpha-1C chain	112	50,590	4.96	12	nanoLC-LTQ Orbitrap XL
		↓	VAT1_RAT	Q3MIE4	Synaptic vesicle membrane protein VAT-1 homolog	110	43,319	6.17	28	nanoLC-LTQ Orbitrap XL
		↓	EF1G_RAT	Q68FR6	Elongation factor 1-gamma	108	50,371	6.31	17	nanoLC-LTQ Orbitrap XL
		↓	TBB2B_RAT	Q3KRE8	Tubulin beta-2B chain	104	50,377	4.78	19	nanoLC-LTQ Orbitrap XL
700	2.8		TPIS_RAT	P48500	Triosephosphate isomerase		26,849	7.29	23.0	nanoLC-LTQ Orbitrap XL
773		↓	ARP2_RAT	Q5M7U6	Actin-related protein 2	267	44,990	6.30	42.4	nanoLC-LTQ Orbitrap XL
		↓	F1LPS8_RAT	F1LPS8	Transcriptional activator protein Pur-alpha	116	34,976	6.07	17.4	nanoLC-LTQ Orbitrap XL
810					n/d					nanoLC-LTQ Orbitrap XL
819	2.6	↓	NDUAA_RAT	Q561S0	NADH dehydrogenase [ubiquinone] 1 alpha subcomplex subunit 10, mitochondrial	542	40,753	7.64	52.0	nanoLC-LTQ Orbitrap XL
		↓	TALDO_RAT	Q9EQS0	Transaldolase	76	37,608	6.57	19.0	nanoLC-LTQ Orbitrap XL
		↓	ALDOC_RAT	P09117	Fructose-bisphosphate aldolase C	76	39,658	6.67	18.0	nanoLC-LTQ Orbitrap XL
		↓	ICA1L_RAT	Q6RUG5	Islet cell autoantigen 1-like protein	43	48,644	5.01		nanoLC-LTQ Orbitrap XL
848	2.1	↑	AK1A1_RAT	P51635	Alcohol dehydrogenase [NADP+]	340	36,506	7.36		MALDI-TOF/TOF
1048	2.0	↓	CAPZB_RAT	Q5XI32	F-actin-capping protein subunit beta	813	30,952	5.69	63.2	nanoLC-LTQ Orbitrap XL
1088	3.9	↓	PA1B2_RAT	O35264	Platelet-activating factor acetylhydrolase IB subunit beta	121	25,736	5.57	13.5	nanoLC-LTQ Orbitrap XL
		↓	H2A1C_RAT	P0C169	Histone H2A type 1-C	88	14,097	11.05	21.5	nanoLC-LTQ Orbitrap XL
1184	2	↑			n/d					
1379	2.1	↑	PRDX5_RAT	Q9R063	Peroxiredoxin-5, mitochondrial	177	22,507	8.94	45.0	nanoLC-LTQ Orbitrap XL
1503	2.1	↓	PEBP1_RAT	P31044	Phosphatidylethanolamine binding protein 1, isoform CRA_b		20,801	5.58		nanoLC-LTQ Orbitrap XL
1591	2.1	↑	PIMT_RAT	P22062	Protein-L-isoaspartate(D-aspartate) O-methyltransferase	120	24,683	7.14	45.0	nanoLC-LTQ Orbitrap XL
1599	2.6	↑	GDIA_RAT	P50398	Rab GDP dissociation inhibitor alpha	1461	51,074	5.00	69.1	nanoLC-LTQ Orbitrap XL
	2.6	↑	PACN1_RAT	Q9Z0W5	Protein kinase C and casein kinase substrate in neurons protein 1	102	50,760	5.15	25.0	nanoLC-LTQ Orbitrap XL
		↑	Q5XI34_RAT	Q5XI34	Protein Ppp2r1a	195	65,323	5.11	53.3	nanoLC-Orbitrap Velos Pro MS
		↑	FETUA_RAT	P24090	Alpha-2-HS-glycoprotein, isoform CRA_b		38,002			nanoLC-LTQ Orbitrap XL
1664	2.0	↑	KCNS1_RAT	O88758	Potassium voltage-gated channel subfamily S member 1	22	54,914	7.66	45.0	MALDI-TOF/TOF
		↑	KPYM_RAT	P11980	Isoform M2 of Pyruvate kinase isozymes M1/M2	330	58,294	6.63	45.0	nanoLC-Orbitrap XL
		↑	KPYR_RAT	P12928	Pyruvate kinase isozymes R/L	64	62,504	6.45	4.9	nanoLC-Orbitrap XL
		↑	EF1A1_RAT	P62630	Elongation factor 1-alpha 1	63	50,424	9.1	2.4	nanoLC-Orbitrap XL
1670		↑			n/d					nanoLC-LTQ Orbitrap XL
1675	2.4	↓	PDIA3_RAT	P11598	Protein disulfide-isomerase A3	751	57,044	5.88	49.1	nanoLC-LTQ Orbitrap XL
		↓	PRS4_RAT	P62193	26S protease regulatory subunit 4	295	49,325	5.87	18.0	nanoLC-LTQ Orbitrap XL
		↓	PPP5_RAT	P53042	Serine/threonine-protein phosphatase 5	108	57,507	5.84	9.6	nanoLC-LTQ Orbitrap XL
		↓	PTMA_RAT	P06302	Prothymosin alpha	79	12,375	3.75	13.0	nanoLC-LTQ Orbitrap XL
		↓	HSPB1_RAT	P42930	Heat shock protein beta-1	62	22,936	6.12	4.9	nanoLC-LTQ Orbitrap XL
1716	3.1	↑(D21); ↓(D3,D7)			rCG57843, isoform CRA_a	1	17,283			nanoLC-LTQ Orbitrap XL
		↑(D21); ↓(D3,D7)	NDKB_RAT	P19804	Nucleoside diphosphate kinase	1	17,283	7.57		nanoLC-LTQ Orbitrap XL
		↑(D21); ↓(D3,D7)	KPYM_RAT	P11980	Pyruvate kinase isozymes M1/M2	6	57,818	7.50		nanoLC-LTQ Orbitrap XL

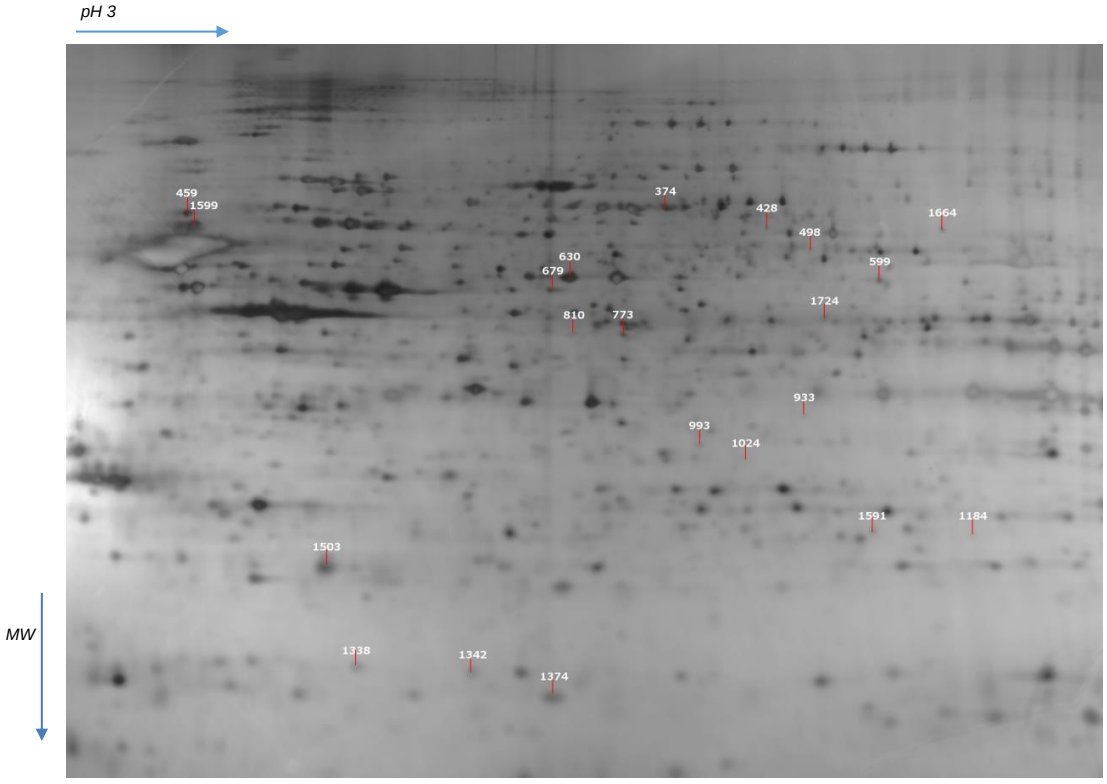

Figure 4. 2D-gel of the left-side CeA. Arrows indicate spots with fold change ≥ 2, when 2D-gels of naïve compared to 2D-gels of neuropathic pain model rats at day 3, 7 and 21 post SNT surgery. The first dimension, an isoelectric focusing (IEF), was perfomed with a immobilised pH gel (pH 3-11NL) of 24 cm long. The second dimension, SDS-PAGE, was perfomed with a 12% SDS polyacrylamide gel.

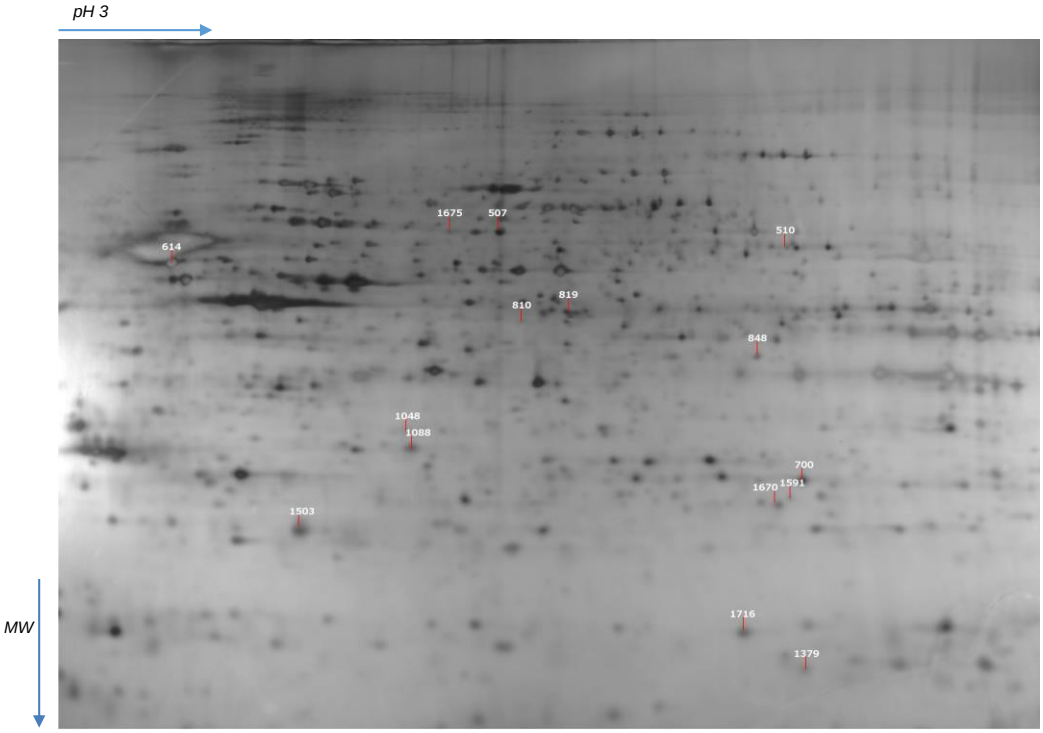

Figure 5. 2D-gel of the right-side CeA. Arrows indicate spots with fold change ≥ 2, when 2D-gels of naïve compared to 2D-gels of neuropathic pain model rats at day 3, 7 and 21 post SNT surgery. The first dimension, an isoelectric focusing (IEF), was perfomed with a immobilised pH gel (pH 3-11NL) of 24 cm long. The second dimension, SDS-PAGE, was perfomed with a 12% SDS polyacrylamide gel.

The intensities of fourteen spots were significantly different and the protein identities of thirteen spots were revealed by nano-LC-MS/MS and MALDI-TOF/TOF analyses when we compared the right-side of CeA of sham versus the right-side of CeA at days 3, 7 and 21 after SNT surgery 2D-gels (Figure 5). Eight spots generated high intensities under the spots for day 3, 7 and 21 SNT models versus sham. More than two proteins were identified for five spots, which showed higher intensities under the spot versus the same spot from sham 2D-gel. Some up-regulated proteins are as follows: ATP synthase subunit ß, synaptosomal-associated protein 29 (spot 614);

nucleoside diphosphate kinase (spot 1716); protein disulphide isomerase A3 (spot 507); perodoxin 5 (spot 1379). Perodoxin 5 is a novel thioredoxin peroxidase recently identified in a variety of human cells and tissues, which is considered to play an important role in oxidative stress protection mechanisms. L-isoapartyl/D-aspartyl O-methyltransferase (PIMT) was up-regulated in the right-side of CeA SNT models (spot 1591). The PIMT protein exhibits high activity in the brain, relative to other tissues and is a putative protein repair enzyme, which converts L-isoaspartyl residues in damaged proteins to normal L-aspartyl residues. PIMT-deficient mice manifested neurodegenerative changes due to the accumulation of L-isoaspartate in the brain [33]. Spot 1670 was identified as protein-L-isoaspartate (D-asparate) O-methyltransferase and was also up-regulated in group 2. Five proteins were significantly down-regulated ($F \geq 2$, $p < 0.1$) in the right-side CeA of day 3, 7 and 21 after SNT surgery rats, including phosphatidylethanolamine binding protein 1 in spot 1503; platelet-activating factor acetylhydrolase IB subunit ß in spot 1088; F-actin-capping protein subunit ß in spot 1048; and for another two spots 1675 and 819 more than two proteins were identified under the spot. Phosphatidylethanolamine-binding protein binds ATP, opioids and phosphatidylethanolamine and previously reported to be associated with memory and learning disorder [34]. Some proteins such as that contained in spots 1675 and 819 are represent trains of similar molecular weight with different *pI*s, which might be derived from post-translational modifications such as phosphorylation events. Two spots (1591 and 1503) were with more than 2-fold change in the left- and right-sides of CeA.

The differentially expressed proteins were annotated in public repositories data by Gene Ontology (GO) terms. Proteins are described by GO terms as biological process, cellular components and molecular function. Figure 6 represents proteins annotated according to their molecular functions compare to an entire rat proteome. Approximately 83% of all identified proteins had protein binding function, 76% catalytic activity, 31% nucleotide binding, 28% metal ion binding and 7% transporter activity. GO biological process annotation analysis revealed that more than 78% of proteins were involved in metabolic process, regulation of biological process and response to

stimulus. Approximately 22% of all identified proteins were involved in transport, development and cell organisation and biogenesis.

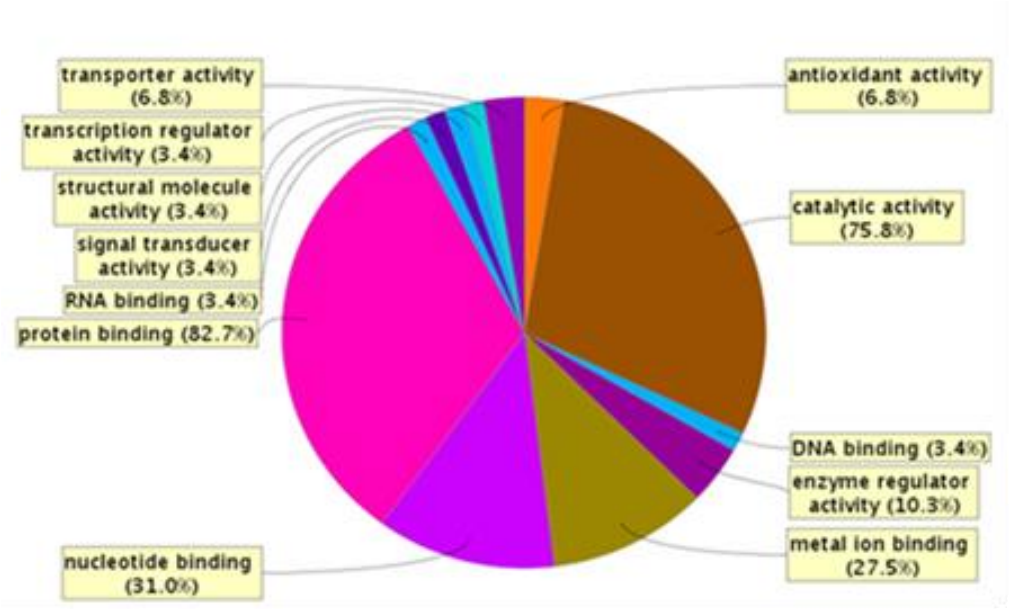

Figure 6. Breakdown of differentially expressed proteins according to molecular function for groups 1 and 2. Differentially expressed proteins at day 7 and 14 after SNT surgery were uploaded to Protein Center and annotated according to Gene Ontology terms.

Membrane proteins mass spectrometry-based proteomics

Membrane proteins are key regulators of crucial processes including the passage of information and substances between cells and mediating activities such as hormone action and nerve impulses. Membrane proteins are scarcely soluble in the buffers used during isoelectric focussing due to the exposure of hydrophobic amino acids on their quaternary structure, leading to a partial extraction of certain species or complete absence from the final gel. Therefore, we pre-fractionated proteins with sodium carbonate washes and obtained crude membrane fractions. We utilised two approaches in this work:- (a) 1D-PAGE combined with nano-LC-MS/MS analysis for

identification of a high molecular weight proteins (b) stable isotope dimethyl labelling of quantitation of membrane proteome in SNT models.

1-SDS-PAGE identification of membrane proteins

We utilised 1-SDS-PAGE methodology combined with nanoLC-MS/MS analysis for the identification of the membrane proteins. The membrane fraction consisting of membrane and membrane associated proteins from sham animals was prepared by the differential centrifugation. Sample were solubilised in a buffer containing 4% SDS. The presence of strong detergent SDS ensured practically complete solubilisation of membrane proteins. Five bands of approximately equal size covering the molecular weight range of 80 to 230 kDa were cut out from SDS-PAGE (Figure S3) and subjected to in-gel digestion with trypsin. The resultant peptides were extracted and analysed by the nano-LC-MS/MS. To identify the proteins present, the MS/MS spectra were submitted to the Mascot algorithm. Mascot then identified the tryptic peptides by matching their MS/MS spectra against *in-silico* generated theoretical spectra from the database. A single run on the LTQ-Orbitrap instrument identified approximately 800 proteins. The combination of our sample preparation procedure with high resolution MS analysis yielded a large number of brain-specific proteins. These include neurotransmitter receptors such as glutamate and GABA receptors and also ion channels such as sodium and potassium channel proteins. The identified glutamate receptors represent NMDA, Glutamate receptor epsilon-1, and Metabotropic glutamate receptor 3. Voltage-dependent ion channels identified include: potassium voltage-gated channel subfamily A member 3, voltage-gated calcium channel alpha2/delta-1 subunit, sodium channel protein type 2 subunit alpha, Nav 1.2, potassium voltage-gated channel subfamily A member 4.

Membrane proteins quantification using stable isotope dimethyl label mass spectrometry technology

We utilised triplex stable isotope dimethyl labelling method, and performed at the peptide level in this work. Triplex stable isotope dimethyl labelling is based on the reaction of peptide primary amines with formaldehyde to generate a Shiff base that is rapidly reduced by the addition of

cyanoborohydride to the mixture [17]. A mass increase of 32 Da per primary amine is achieved using deuterated formaldehyde ("intermediate" label). By combining deuterated and ^{13}C-labeled formaldehyde with cyanoborodeuteride, we achieved the third label with a mass increase of 36 Da ("heavy" label). We employed *on-column* stable isotope dimethyl labelling to differentially label three samples to allow simultaneous quantitative LC-MS analysis. We used trypsin as the enzyme for digestion of proteins; this cleaves C-terminal of lysine and arginine residues. We performed the trypsin digestion in buffer without primary amines in triethyl ammonium bicarbonate (TEAB) buffer, because this method might be prone to contaminating and interfering components remaining after sample preparation. These components might include primary amine-containing molecules such as ammonium bicarbonate or Tris. As formaldehyde will also react with these amines, these compounds affect the labelling efficiency. Followed by de-salting the peptide sample before labelling using self-made µC18 columns, peptides of the different samples were separately on-column labelled with either of the dimethyl isotopomers, and the final eluents from three µC18 StageTips were combined. This protocol was optimised for sample amount of 15 µg using a 3 mg of 3cc C_{18} SepPak stationary phase packed into a 10-µL tip [17, 35, 36]. In MS, the different stable isotopically labelled peptides are measured and these peptides are recognised by the known mass difference between them. When labelling the tryptic peptides with this method most peptides differ in mass by either 4 Da (when cleaved after an arginine residue, only the N terminus is labelled) or 8 Da (when cleaved after a lysine residue, both the N terminus and the lysine. Both the peptide N termini and lysine residues are labelled) between the light and intermediate and between the intermediate and heavy label. Our samples of which peptides were differentially stable isotope dimethyl labelled by the on-column protocol were separated by a 290 min gradient on a nano- LC reversed phase column. This way, more peptides were identified and quantified as the total MS time was increased and peptides were better resolved. We employed relatively long columns and small particle sizes (50 cm, 1.8 µm) to facilitate deep sampling of the proteome. We found the combination of a 50-cm column and nearly 5-hour gradient to be a good combination for standard use. We utilised a Q Exactive™ mass spectrometer, which is capable of determining peptide precursor charge states and fully resolving all peaks with high-resolution

(for example, resolution more than 90,000 was achieved at *m/z* 524). Therefore, the *m/z* of the labelled peptides was measured with this high resolution, and peptides ions were selected for fragmentation (MS/MS) to determine the amino-acid sequence. After the LC-MS/MS run, these tandem MS spectra were matched against theoretical spectra obtained from a protein sequence database using Mascot algorithm, which was capable of identifying differentially stable isotope dimethyl-labelled peptides. Quantification was achieved by comparing the intensities of the differentially labelled peptides at MS level, integrated with their extracted ion chromatograms using Proteome Discovery software.

Adult rat CeA is a small brain region which possibly contains about 1 mg of wet tissue and around 80 - 100 µg of total protein mass. Therefore, in depth analysis of the CeA membrane proteome of one single rat is required precise analytical method. Before applying this technology to SNT samples, we analysed control samples to validate the protocol. A BSA digest (5 µg protein per label) was dimethyl labelled in a 1:1:1 light/medium/heavy ratio. An *m/z* shift compared with the non-labelled peptide (*m/z* 927.6) of respectively, 28.03, 32.06 and 36.08 were found for the light, intermediate and heavy peptide ions, respectively (Figure 7). As the peptide ions are doubly charged, these *m/z* shifts correspond to mass increments of respectively 56.06, 64.11 and 72.15 Da. This is consistent with the fact that the peptide has two sites available to be labelled, the N terminus and the lysine residue. Complete labelling was obtained as no peaks at the *m/z* corresponding to unlabelled peptides was observed in the dimethyl-labelled sample. The sample was analysed in triplicate by nano-LC-MS/MS. The LC-MS/MS files were combined and analysed by Proteome Discoverer 1.3 Thermo Scientific. Mascot identified peptides, which accounts for 95% of the sequence BSA (Swiss-Prot-UniProt, P02769) and none of non-labelled peptides were identified upon database searching with Mascot.

To validate the protocol further, we prepared membrane fractions from sham and neuropathic pain model rats at day 7 and 21 after SNT surgery using Na_2CO_3 washes and the resulting membrane pellets were solubilised in 0.2% ProteaseMax Surfactant in 50 mM TEAB. ProteaseMax Surfactant (molecular weight 451.51 Da) was a good detergent to solubilise

membrane proteins. It is designed to degrade over the course of a trypsin digestion reaction and completely degraded with an addition of 5% acetic acid, just before on-column dimethyl labelling, producing a hydrophilic zwitterionic species (molecular weight 139.17 Da) and neutral hydrophobic species (molecular weight 238.36 Da), which do not interfere with mass spectrometry analysis at that concentration. After protease digestion, this sample (~15 µg of protein) was split in three equal portions and the peptides were on-column differentially stable isotope dimethyl labelled in a 1:1:1 ratio light/medium/heavy ratio and mixed. We use approximately 5 µg of protein per label. In the first instance for checking the quality of our samples we analysed this sample by MALDI-TOF/TOF. A ratio of 1:1:1 was obtained for ~97% of triplex isotope dimethyl labelled peptides. The labelled peptide mixtures were then loaded separately onto the autosampler of the nano-LC system (Ultimate 3000) and analysed in an automated manner by nano-LC-MS/MS on a Q Exactive mass spectrometer. The addition of three dimethyl labels makes the peptide more hydrophobic, thereby increasing its retention on the nano-C18 column. A slight separation was observed between the differently labelled species of the same peptide. Using Proteome Discoverer software and stringent filtering criteria as described in method section, we quantified around 650 proteins per one LC-MS/MS run. We combined three technical nano-LC-MS/MS runs of the same sample we quantified around 1300 proteins. The performance of the dimethyl labelling experiment was found to be around 80% of the identified proteins quantified.

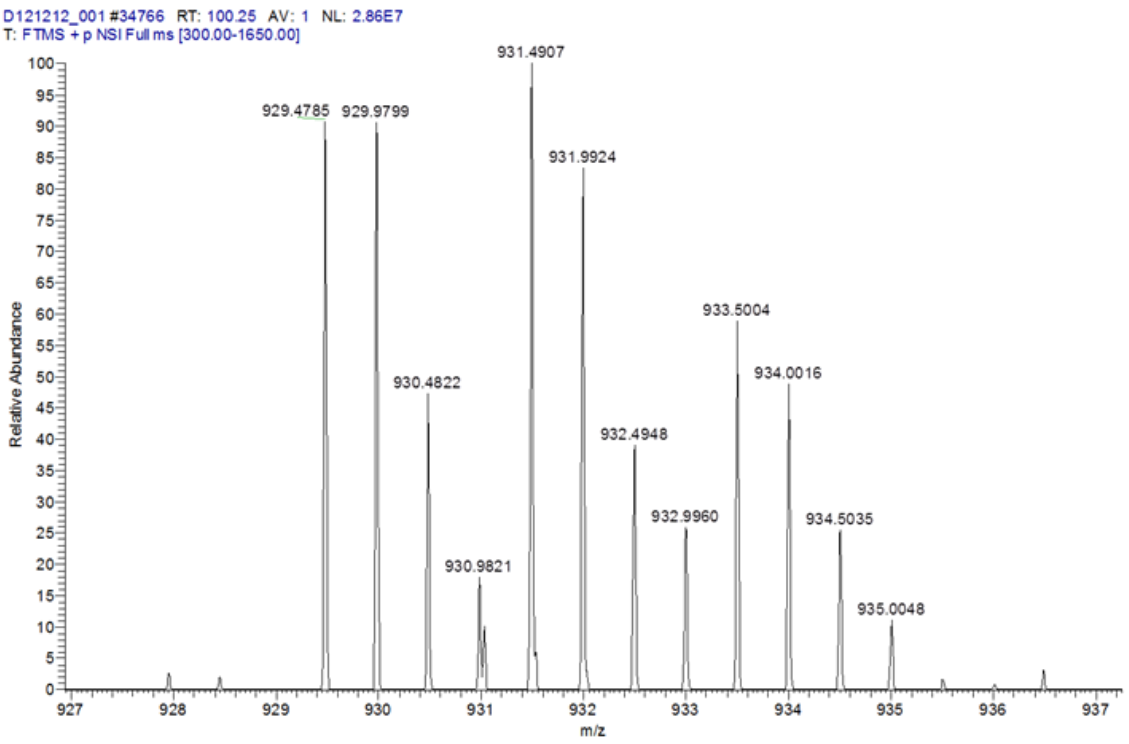

Figure 7. Mass spectrum of the triplex stable isotope dimethyl labelled peptide. Light , intermediate and heavy labelled peptides shifted by 28.03; 32.06 and 36.08 *m/z,* corresponding to 56.06, 64.11 and 72.15 Da as the peptide ion is doubly charged. This peptide is dimethyl labelled on one site showing *m/z* difference of 2.01.

Around 3 µg of membrane proteins from CeA of sham and rats at day 3, 7 and 21 after SNT surgery were reduced/alkylated, in-solution digested with trypsin, and the resulting peptides were purified on µC18 Stage Tips and triplex dimethyl labelled with light, medium and heavy-tags, following by 1:1:1 mixing. We used two biological samples. Samples were analysed by nano-LC-MS/MS using the 5-h gradient. We analysed each sample in triplicate by the LC-MS/MS. Proteome Discoverer software incorporated with Mascot was used to identify and quantify peptides and proteins. The combination of the data generated from mixture 1 samples allowed the cumulative quantification of more than 1,300 protein groups, 6,000 merged proteins, 4,500 peptides and 110,000 PSMs (FDR < 0.5%), and around 950 proteins were quantified per each ratio either Heavy/Light or Medium/Light. Next, we filtered our data sets to keep only proteins

found in both biological samples and calculated their median isotopic ratios (heavy (SNT day 21)/ light (sham); medium (SNT day 3)/ light (sham); medium (SNT day 7)/ light (sham) and duplicate ratios generated from mixture 1 and 2 samples of heavy (SNT day 21) / light (sham) were combined (Figure 8).

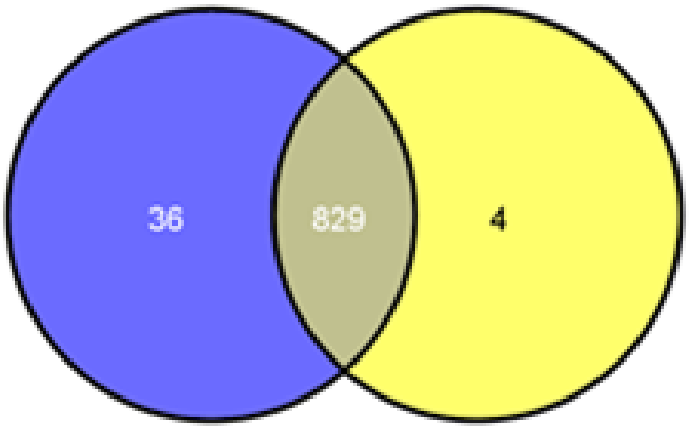

Figure 8. Venn diagram shows quantified proteins in Mixture 1 and Mixture 2 samples for Heavy/Light ratio.

Doublecortin (DCX) was quantified as one of the proteins significantly up-regulated in membrane fractions of CeA of rats at 3, 7 and 21 days post SNT surgery compared to sham, with sequence coverage of around 50% and 6 peptides were taken for quantification analysis. Figure 9 shows MS/MS spectrum of *m/z* 724.9130 corresponding to doubly charged peptide NVNPNWSVNVK, which was dimethyl labelled on two sites.

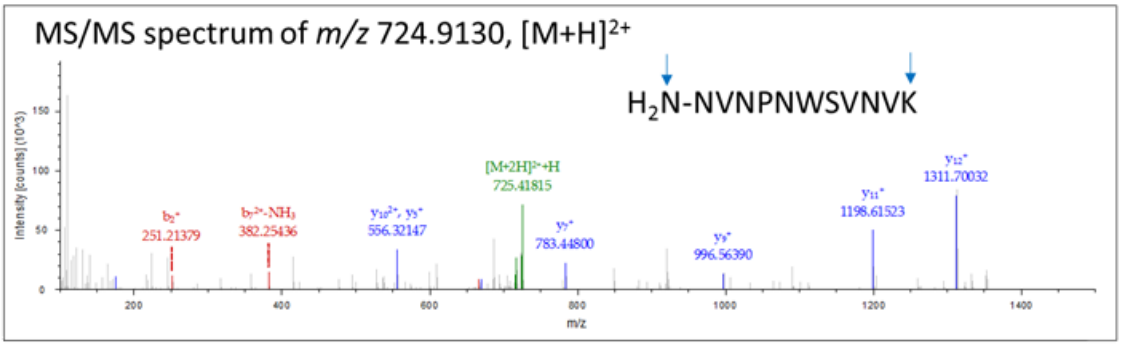

Figure 9. MS/MS spectrum of *m/z* 724.9130 $[M+H]^{2+}$ ion corresponding to peptide NVNPNWSVNVK, which was dimethyl labelled on two sites.

DCX is microtubule-associated protein required for initial steps of neuronal dispersion and cortex lamination during cerebral cortex development [37]. This protein may act by competing with the putative neuronal protein kinase DCLK1 in binding to a target protein and may in that way participate in a signalling pathway that is crucial for neuronal interaction before and during migration, possibly as part of a calcium ion-dependent signal transduction pathway. It also found to participate along with PAFAH1B1/LIS-1 in a distinct overlapping signalling pathway that promotes neuronal migration.

Validation of altered expression levels by Western blotting

Western blotting revealed that the expression level of DCX was localised in the CeA tissue lysate and was of equal amount in CeA of sham and neuropathic animals (Figure 10b). Consistent with the mass spectrometry findings, DCX was detected in the membrane fractions of CeA in neuropathic model animals but not in sham (Figure 10a). Immunoblot analysis showed a significant increase in the levels of DCX in membrane fraction in CeA of animals at day 21 after SNT surgery confirming mass spectrometry data.

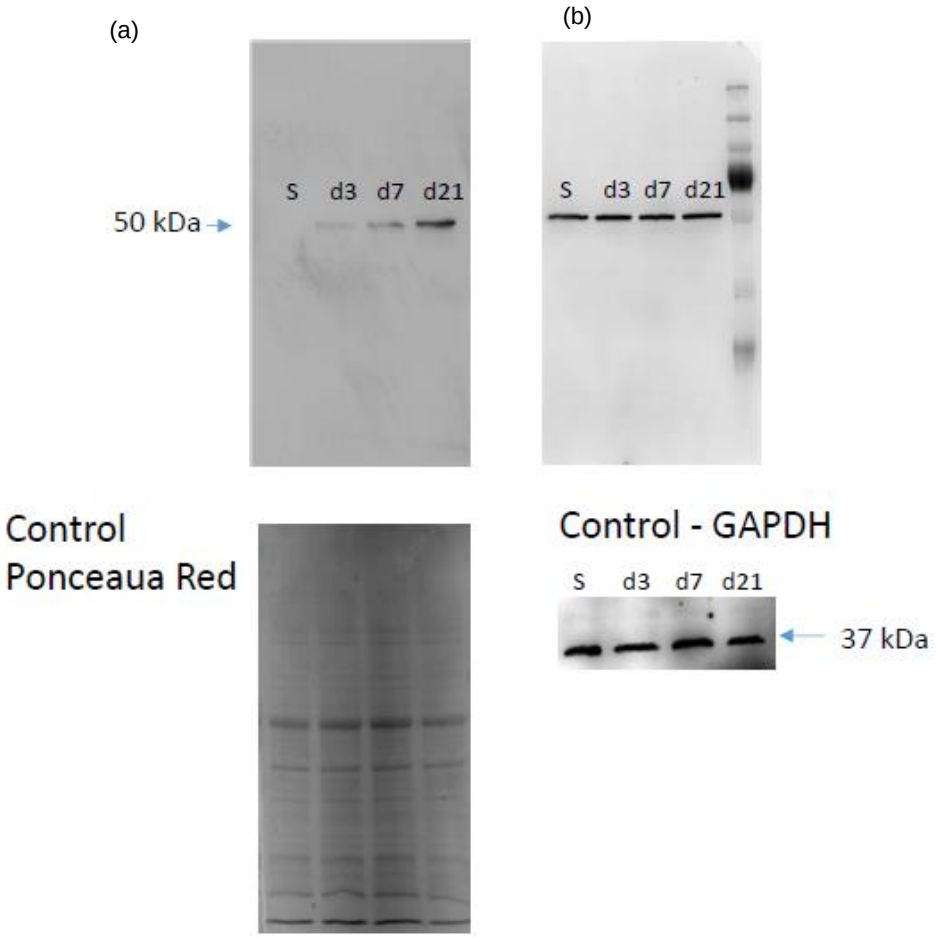

Figure 10. Western blots of CeA (a) the protein content of DCX in membrane fractions of CeA from sham and neuropathic pain rats at day 3, 7 and 21 after SNT surgery. Equal amounts of protein were loaded onto the gel followed by SDS-PAGE gel electrophoresis, immunoreaction. (b) The protein content of whole tissue lysate shows that DCX in CeA did not differ in sham and neuropathic pain models.

Immunohistochemistry of DCX in CeA of Sham and SNT model rats

By using triple labelling fluorescence experiment performed with DCX and 58k Golgi protein antibodies plus DAPI to localise DCX in the CeA of sham animal. Figure 11 shows triple staining using 58K Golgi maker and DAPI of a 10 µm brain section from sham animal, co-stained for DCX. DCX displayed co-localisation with 58K Golgi protein indicating the presence of DCX in the Golgi

apparatus. Triple immunofluorescent labelling was repeated for rats at 7 and 21 days post SNT and revealed that DCX and the Golgi marker were not co-localised. We also studied a localisation of DCX at the plasma membranes. Colocalization of DCX with α1 Na/K-ATPase subunit and DAPI was examined in the CeA of sham and rats at 7 and 21 days post SNT surgery. α1 Na/K-ATPase subunit antibody was used as a plasma membrane marker. We observed that DCX is present in processes of CeA in these SNT model animals and co-localises with the plasma membrane marker, α1 Na, K-ATPase (Figure 12), but not in CeA of sham. Together, the DCX distribution by immunohistochemistry showed that DCX is expressed in processes in CeA of rats 7 and 21 days post SNT surgery. This suggests that doublecortin contributes to the neuronal plastic changes in CeA in neuropathic pain models.

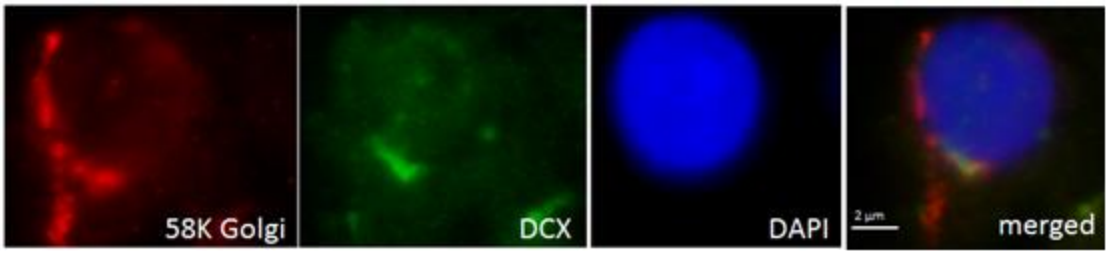

Figure 11. In CeA of sham, DCX (green) is found along with 58K Golgi protein and co-localises to the Golgi apparatus as shown by co-localisation with a Golgi marker and DCX.

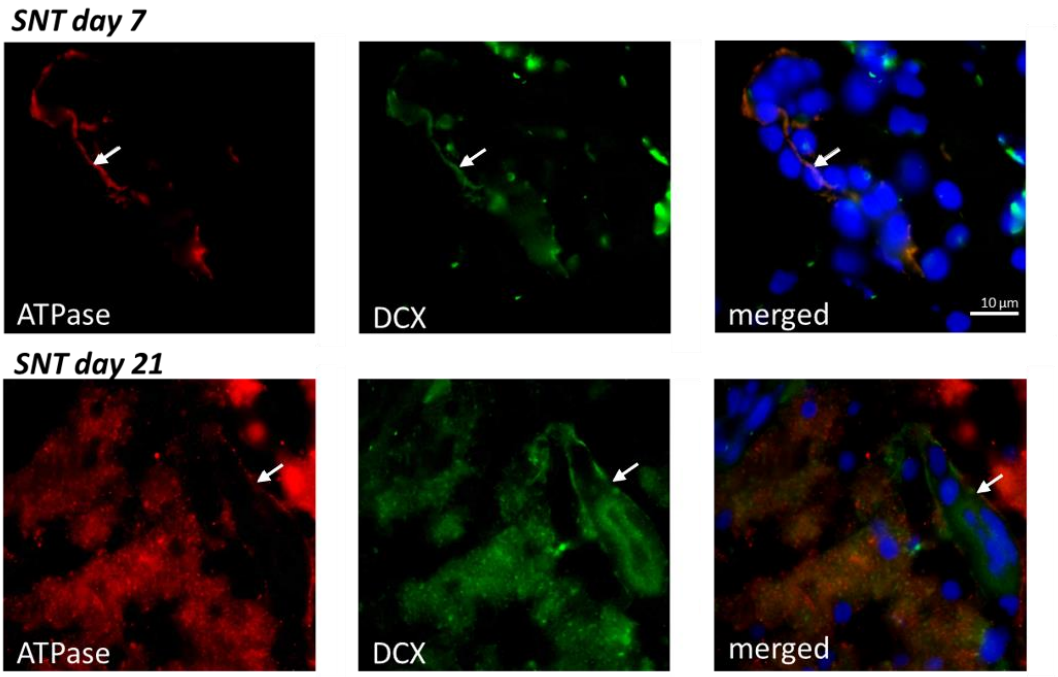

Figure 12. Representative immunohistochemical images from the CeA of rats at day 7 and 21 post SNT surgery demonstrating co-labelling with DCX (green) and ATPase (red), respectively. The sections are counterstained with DAPI nuclear marker.

Validation of differentially expressed proteins by real-time PCR for Group 2 SNT models

To verify the reliability of the proteomics analysis, we selected central amygdala differentially changed twenty six genes at day 21 after SNT surgeries for quantitative real-time PCR analysis.

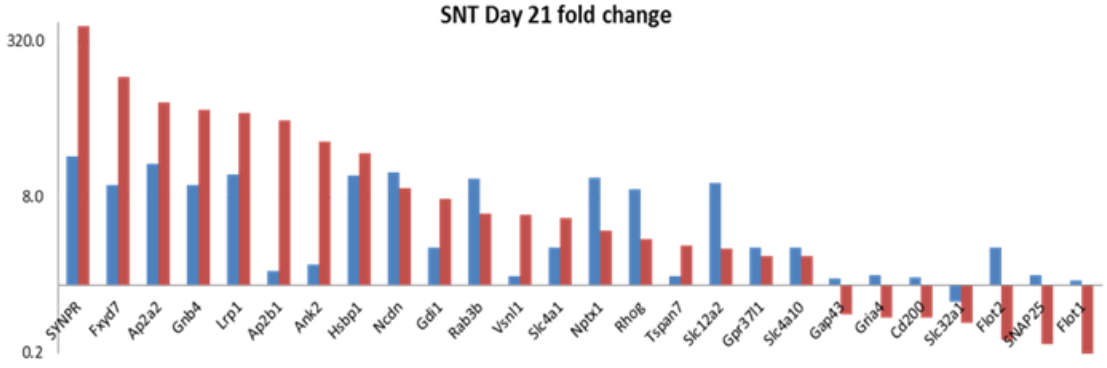

Figure 13. Expression changes of selected genes in the CeA of rats at days 21 after SNT surgery by quantitative real-time PCR and by 2D-electrophoresis as compared to sham. Red bar represent cDNA fold change normalised to yWHAZ and blue bars represent protein fold change.

The mRNA levels of nineteen genes followed the same up-regulation trend after SNT surgery in comparison to sham supporting proteome data ($p<0.05$), while for five genes mRNA expression levels were down-regulated in rats at day 21 after SNT surgery. It is likely that this relates to mRNA-independent post-translational modification, trafficking and degradation, as a large number of modification sites and domains. However, this could also be due to qPCR experiments were carried out using cDNA extracted from whole CeAs. Figures 13 shows the proteome and transcriptome fold changes in neuropathic pain rats at day 21 post SNT surgery.

Discussion

We know that peripheral nerve injury could lead to altered regulation of a large number of molecules. Several gene array studies and proteomics studies have been directed to investigate the genes regulated in CNS following nerve injury. A recent report by Wu et al. showed effects of electro-acupuncture stimulation on protein levels in amygdala of complete Freund's adjuvant-induced inflammatory pain model rats using iTRAQ labelling [38]. They showed more than 100 altered proteins in the painful condition, and this proves the hypothesis that plastic changes occur in amygdala in pain conditions, albeit they used the entire amygdala rather than focusing on CeA.

In this study, we performed proteomics investigation of neuropathic CeA using the spinal nerve transection model in which animals developed signs of neuropathy at days 7 and 14 (group 1), and at days 3, 7 and 21 (group 2) post-transection of L5 spinal nerve. In both groups, we found CeA proteome changes in a complex asymmetrical and time-related manner following neuropathy.

We identify more 50 proteins in the right-side of CeA and around 45 proteins in the left-side of CeA in group 1. Those differentially expressed proteins are involved in physiological, metabolic

and cellular processes and development processes. In summary many identified proteins involved in neural plasticity/neurotransmitter release were either up-regulated in the right-side of CeA after SNT surgery (e.g. Cofilin-1, Syntaxin-1A) and down-regulated in the control side (e.g. F-actin-capping protein α-2, Transgelin-3). Multiple subtypes of Ras-related protein Rab (involved in protein transport) were up-regulated in the right-side of CeA after SNT surgery. Both alpha- and gamma-enolase (suggested to be involved in cell survival) were down-regulated in the right-side of CeA after SNT surgery, while Protein DJ-1 (protects neurons against oxidative stress and cell death) were up-regulated.

We observed decrease in mitogen-activated protein kinase in the right-side of CeA. Mitogen-activated protein kinases, including extracellular signal-regulated kinase, mediate plasticity in the amygdala and hippocampus. Creatine kinase B was decreased after nerve injury in both-sides of CeA in this study. Creatine has been found to reduce glutamate levels and to exhibit neuroprotective properties [39]. Therefore, the down-regulation of creatine kinase B might be particularly important for the development and maintenance of neuropathic pain. Gamma-enolase was up-regulated in rats at day 7 abut down-regulated in rats at day 14 post SNT surgery. Neuronal gamma-enolases exists in the synaptic plasma membrane (Komori, 2011) and may interact with creatine kinase and pyrivate kinase and were identified in the right-side of CeA, but not in the left-side. Calcium/calmodulin-dependent protein kinase type II subunit alpha was down-regulated the right-side of CeA in neuropathic pain rats α-CaMKII is a critical contributor to the spontaneous/ongoing component of tissue-injury evoked persistent pain. Dual specificity mitogen-activated protein kinase kinase (MAPKs) plays critical roles in regulating neural plasticity and inflammatory responses. Vesicle-fusing ATPase N-ethylmaleimide-sensitive fusion protein (NSF) was down-regulated in the left-side of CeA 14 days after surgery but up-regulated at day 7. This protein was reported to be involved in central sensitisation in the spinal cord through GluR2 subunit composition switch after inflammation. Protein L-isoaspartyl methytransferase was up-regulated in neuropathic pain rats at 7 day but down-regulated in day 14 after surgery, with no

difference between the left and right CeA. This protein catalyses repair of L-isoaspartyl peptide bonds, a major source of protein damage under physiological conditions.

We concluded that asymmetric changes in proteome were observed with the right-side of CeA dominating. Also, protein change in the right-side of CeA was higher at day 14 after surgery, and differences between the left- and right-sides of CeA proteome change was in all groups.

Even through the group 2 consisted of different days post SNT surgeries, we identified around twenty proteins, which were up- or down-regulated in the left- and the right-side of CeA as in group 1. For example:- gamma-enolase, creatine kinase, pyruvate kinase M1 and M2, glycolytic enzymes, trasgelin-3, perodoxin-6, dual specificity mitogen-activated protein kinase kinase 1, pyruvate kinase, phosphatidylethanolamine-binding protein 1, protein L-isoaspartyl methytransferase, triosepthishate isorase, heat shock 60 and 90. ATP synthase subunit α. These regulated identified proteins function in diverse pathways such as inflammation, cellular metabolic enzymes, proteins in defence against oxidation and neuronal cell death, membrane-associated proteins in signal transduction. This could be explained that in the nervous system, nerve injury and stress can cause oxidative damage to the cytoskeleton and membrane structures. In addition, significant energy production is required for protein expression and cellular defence mechanisms. This is supported by the increased expression of proteins involving antioxidative processes, neuronal integrity and glycolysis/gluconeogenesis observed in this work. The expression of thirty-five differential proteins was further examined using quantitative real-time PCR. In overall, we found changes were similar to that for 2D electrophoresis and only few gene expression levels were not correlated to mRNA levels. It is likely that this relates to mRNA-independent post-translational modification, trafficking and degradation, as a large number of modification sites and domains.

In conclusion, we observed the regulation of a large population of proteins in cellular defence mechanisms and antioxidation. The up-regulation of many proteins in the actin cytoskeletal

organisation strongly suggests the concept that stabilisation of actin cytoskeleton is one of the priorities in a fight against injury or stress [40, 41]. Nearly half of the proteins that we identified in this study have been shown to be similarly regulated at the mRNA levels or proteins levels after other types peripheral nerve injury, validating our experimental procedures.

There are several notable limitations to this study. First, proteome quantification by silver staining has several issues as a standard quantification (e.g. poor linear dynamic response, non-specific staining of nucleic acids and lipopolysaccharides, non-sensitivity in detecting certain proteins) (Gauci *et al.* 2011). In order to mitigate these issues, each sample was run in triplicate and the relative quantification of a spot was calculated as the mean of its relative volumes; the mean coefficient of variation (CV) for these relative volumes was 20% (±5%). Based on this finding, only a protein expression ratio of less than 1.5 can be empirically deemed experimental variation. Therefore, only proteins spots those were up-regulated or down-regulated by at least 2.0-fold with $p < 0.1$ were considered significantly differentiated. The most important drawback of gel-based and mass spectrometry-based proteomics is that it is not possible to analyse the entire proteome. Proteins displayed in a single 2D-gel represent only a portion of the proteins in a sample, and low-abundance proteins such as regulatory proteins and receptors are often not detected by conventional staining. Membrane proteins are not readily amenable to 2-DE due to their poor solubility in standard protein extraction solutions [42, 43]. Therefore, our study could only identify a limited set of differentially expressed proteins after SNT surgery.

Quantification of membrane proteome of CeA from neuropathic pain model animals

Membrane proteins are key regulators of crucial processes including the passage of information and substances between cells and mediating activities such as hormones action and nerve impulses. More than 30% of the mammalian genome encodes membrane proteins. These proteins are challenging to study, but essential to understand, as they represent two-thirds of drug targets. Mapping of membrane proteome and identification of drug targets requires methods for tissue extraction, protein processing and sensitive and specific analysis. Taking advantage of

our established membrane purification method for micro-scale identification and quantification of membrane proteins in this work and recent development in high resolution and high accuracy mass spectrometer, we performed an in-depth comparative analysis of membrane proteomes of sham versus neuropathic pain model rats. The CeA amygdala contains around 100 µg of total protein. Therefore, we had a limited amount of membrane proteins from neuropathic pain model rats but despite the mass limitations, we were able to identify as many as 1,300 proteins and quantify around 950 proteins from a single biological analysis. Synaptoporin, syntaxin and sodium channel subunit 1 and metabotropic glutamate receptor were up-regulated at day 3 after SNT surgery. Our findings also support an impairment of synaptic function in CeA, especially for components of soluble N-ethylmaleimide sensitive (NSF) sensitive factor attachment protein receptor (SNARE) function. Syntaxin 6 was unregulated is a cellular receptor for transport vehicle which inhibits SNARE function and thereby controls neurotransmitter release. The endocannabinoid system, which consists of the cannabinoid receptors referred to as CB1 and CB2 [44] and endogenous ligands can regulate pain perception [45]. CB1 receptors are associated with the peripheral and central nervous systems and CB1 agonist have been shown to reduce hyperalgesia in animal models of inflammatory [46], neuropathic [47], capsaicin [48], and cancer pain [49]. CB1 receptor was up-regulated in this study. Neurochodrin was unregulated in SNT model rats and it was previously shown that neurochodrin seems to interact with phosphatidic acid, which is metabolite related to phospholipid metabolism.

DCX was up-regulated in membrane fraction of CeA in SNT model rat. DCX protein associated with immature neuronal phenotypes and elevated neuroplasticity in the adult brain and evidence from the rodent studies suggests that stress may modify their expression in amygdala and was found to be increased in CeA [50]. DCX is mainly found in immature neurons during development of the nervous system and believed to play an important role in neurogenesis, neuromigration, and axon growth. This is why DCX has been widely used as a marker for immature neurons. Interestingly, DCX has been used as a marker for adult neurogenesis as well, typically in hippocampal dentate gyrus and the subventricular zone [51,52]. Such adult neurogenesis in those

regions of brain apparently implicates the impact of neurogenesis in memory formation/learning and the olfactory system. However, recent findings suggest tissues which are previously not strongly linked to neurogenesis have upregulated DCX including dorsal root ganglia [53]. Thus, DCX seems to be involved not only in neurogenesis in developing brain, but also in reformation/rewiring of neurons in multiple tissues such as dorsal root ganglia and central amygdala.

We found that significant increase of DCX in the membrane fraction without changes in total amount of the protein in CeA. DCX is known to associate with microtubules, but it is also reported that DCX associates with membrane bound actin via Spinophilin [54]. Spinophilin is known as actin binding protein but it also binds to some membrane proteins such as G-protein coupled receptors. DCX may link microtubules to actin and other membrane-bound proteins via Spinophilin and promote axonal growth in re-networking of neurons within and beyond CeA in chronic pain conditions.

SUPPORTING INFORMATION:

The following supporting information is available free of charge at ACS website http://pubs.acs.org

Figure S1. Nissl staining image showing rat amygdala

Figure S2. The right-side vs the left-side of CeA of Naïve, day 7, and day 14 post SNT surgery rats

Figure S3. 2D-gel of the left-side CeA

Reference List

1. Neugebauer,V. Amygdala pain mechanisms. *Handb. Exp. Pharmacol.* **227**, 261-284 (2015).

2. Neugebauer,V. & Li,W. Differential sensitization of amygdala neurons to afferent inputs in a model of arthritic pain. *J. Neurophysiol.* **89**, 716-727 (2003).

3. Neugebauer,V., Li,W., Bird,G.C., Bhave,G., & Gereau,R.W. Synaptic plasticity in the amygdala in a model of arthritic pain: differential roles of metabotropic glutamate receptors 1 and 5. *J. Neurosci.* **23**, 52-63 (2003).

4. Goncalves,L. & Dickenson,A.H. Asymmetric time-dependent activation of right central amygdala neurones in rats with peripheral neuropathy and pregabalin modulation. *Eur. J. Neurosci.* **36**, 3204-3213 (2012).

5. Neugebauer,V., Li,W., Bird,G.C., & Han,J.S. The amygdala and persistent pain. *Neuroscientist.* **10**, 221-234 (2004).

6. Iwazaki,T., McGregor,I.S., & Matsumoto,I. Protein expression profile in the amygdala of rats with methamphetamine-induced behavioral sensitization. *Neurosci. Lett.* **435**, 113-119 (2008).

7. Kekesi,K.A. *et al.* Altered functional protein networks in the prefrontal cortex and amygdala of victims of suicide. *PLoS. One.* **7**, e50532 (2012).

8. Maheu,M.E., Davoli,M.A., Turecki,G., & Mechawar,N. Amygdalar expression of proteins associated with neuroplasticity in major depression and suicide. *J. Psychiatr. Res.* **47**, 384-390 (2013).

9. Mann,M. Origins of mass spectrometry-based proteomics. *Nat. Rev. Mol. Cell Biol.* **17**, 678 (2016).

10. Lu,A., Wisniewski,J.R., & Mann,M. Comparative proteomic profiling of membrane proteins in rat cerebellum, spinal cord, and sciatic nerve. *J. Proteome. Res.* **8**, 2418-2425 (2009).

11. Aebersold,R. & Mann,M. Mass-spectrometric exploration of proteome structure and function. *Nature* **537**, 347-355 (2016).

12. Lilley,K.S., Razzaq,A., & Dupree,P. Two-dimensional gel electrophoresis: recent advances in sample preparation, detection and quantitation. *Curr. Opin. Chem. Biol.* **6**, 46-50 (2002).

13. Lilley,K.S. & Dupree,P. Methods of quantitative proteomics and their application to plant organelle characterization. *J. Exp. Bot.* **57**, 1493-1499 (2006).

14. Huang,J.T. *et al.* Independent protein-profiling studies show a decrease in apolipoprotein A1 levels in schizophrenia CSF, brain and peripheral tissues. *Mol. Psychiatry* **13**, 1118-1128 (2008).

15. Iglesias-Gato,D. *et al.* The proteome of prostate cancer bone metastasis reveals heterogeneity with prognostic implications. *Clin. Cancer Res.* **24**, 5433-5444 (2018).

16. Ross,P.L. *et al.* Multiplexed protein quantitation in Saccharomyces cerevisiae using amine-reactive isobaric tagging reagents. *Mol. Cell Proteomics.* **3**, 1154-1169 (2004).

17. Boersema,P.J., Raijmakers,R., Lemeer,S., Mohammed,S., & Heck,A.J. Multiplex peptide stable isotope dimethyl labeling for quantitative proteomics. *Nat. Protoc.* **4**, 484-494 (2009).

18. Ong,S.E. & Mann,M. A practical recipe for stable isotope labeling by amino acids in cell culture (SILAC). *Nat. Protoc.* **1**, 2650-2660 (2006).

19. Ong,S.E. & Mann,M. Identifying and quantifying sites of protein methylation by heavy methyl SILAC. *Curr. Protoc. Protein Sci.* **46**, Unit 14.9.1-12 (2006).

20. Apweiler,R. *et al.* UniProt: the Universal Protein knowledgebase. *Nucleic Acids Res.* **32**, D115-D119 (2004).

21. Apweiler,R., Bairoch,A., & Wu,C.H. Protein sequence databases. *Curr. Opin. Chem. Biol.* **8**, 76-80 (2004).

22. Boateng,E.K., Novejarque,A., Pheby,T., Rice,A.S., & Huang,W. Heterogeneous responses of dorsal root ganglion neurons in neuropathies induced by peripheral nerve trauma and the antiretroviral drug stavudine. *Eur. J. Pain* **19**, 236-245 (2015).

23. Morland,R.H., Novejarque,A., Spicer,C., Pheby,T., Rice,A.S. Enhanced c-Fos expression in the central amygdala correlates with increased thigmotaxis in rats with peripheral nerve injury. *Eur. J. Pain* **20**, 1140-1154 (2016).

24. Perkins,J.R., Antunes-Martins,A., Calvo,M., Grist,J., Rust,W., Schmid,R., Hildebrandt,T., Kohl,M., Orengo,C., McMahon,S.B., Bennett,D.L. A comparison of RNA-seq and exon arrays for whole genome transcription profiling of the L5 spinal nerve transection model of neuropathic pain in the rat. *Mol. Pain* **10-7** (2014).

25. Ji,G. & Neugebauer,V. Hemispheric lateralization of pain processing by amygdala neurons. *J. Neurophysiol.* **102**, 2253-2264 (2009).

26. Ji,G., Horvath,C., & Neugebauer,V. NR2B receptor blockade inhibits pain-related sensitization of amygdala neurons. *Mol. Pain* **5**, 21 (2009).

27. Carrasquillo,Y. & Gereau,R.W. Hemispheric lateralization of a molecular signal for pain modulation in the amygdala. *Mol. Pain* **4**, 24 (2008).

28. Velazquez,K.T., Mohammad,H., & Sweitzer,S.M. Protein kinase C in pain: involvement of multiple isoforms. *Pharmacol. Res.* **55**, 578-589 (2007).

29. Huang,H.L. *et al.* Proteomic profiling of neuromas reveals alterations in protein composition and local protein synthesis in hyper-excitable nerves. *Mol. Pain* **4**, 33 (2008).

30. Joels,G. & Lamprecht,R. Interaction between N-ethylmaleimide-sensitive factor and GluR2 is essential for fear memory formation in lateral amygdala. *J. Neurosci.* **30**, 15981-15986 (2010).

31. Tajika,Y., Sato,M., Murakami,T., Takata,K., & Yorifuji,H. VAMP2 is expressed in muscle satellite cells and up-regulated during muscle regeneration. *Cell Tissue Res.* **328**, 573-581 (2007).

32. Niederberger,E. & Geisslinger,G. Proteomics in neuropathic pain research. *Anesthesiology* **108**, 314-323 (2008).

33. Takahashi,N., Hayano,T., & Suzuki,M. Peptidyl-prolyl cis-trans isomerase is the cyclosporin A-binding protein cyclophilin. *Nature* **337**, 473-475 (1989).

34. Ojika,K. *et al.* Hippocampal cholinergic neurostimulating peptides (HCNP). *Prog. Neurobiol.* **60**, 37-83 (2000).

35. Rappsilber,J., Ishihama,Y., & Mann,M. Stop and go extraction tips for matrix-assisted laser desorption/ionization, nanoelectrospray, and LC/MS sample pretreatment in proteomics. *Anal. Chem.* **75**, 663-670 (2003).

36. Rappsilber,J., Friesen,W.J., Paushkin,S., Dreyfuss,G., & Mann,M. Detection of arginine dimethylated peptides by parallel precursor ion scanning mass spectrometry in positive ion mode. *Anal. Chem.* **75**, 3107-3114 (2003).

37. Fiorentini,A., Rosi,M.C., Grossi,C., Luccarini,I., & Casamenti,F. Lithium improves hippocampal neurogenesis, neuropathology and cognitive functions in APP mutant mice. *PLoS. One.* **5**, e14382 (2010).

38. Wu,Y., Jiang,Y., Shao,X., He,X., Shen,Z., Shi,Y., Wang,C., & Fang,J. Proteomics analysis of the amygdala in rats with CFA-induced pain aversion with electro-acupuncture stimulation. *J. Pain Res.* **12**, 3067-3078 (2019).

39. Genius,J. *et al.* Creatine protects against excitoxicity in an in vitro model of neurodegeneration. *PLoS. One.* **7**, e30554 (2012).

40. Ikeda,H., Tsuda,M., Inoue,K., & Murase,K. Long-term potentiation of neuronal excitation by neuron-glia interactions in the rat spinal dorsal horn. *Eur. J. Neurosci.* **25**, 1297-1306 (2007).

41. Ikeda,R., Takahashi,Y., Inoue,K., & Kato,F. NMDA receptor-independent synaptic plasticity in the central amygdala in the rat model of neuropathic pain. *Pain* **127**, 161-172 (2007).

42. Santoni,V., Kieffer,S., Desclaux,D., Masson,F., & Rabilloud,T. Membrane proteomics: use of additive main effects with multiplicative interaction model to classify plasma membrane proteins according to their solubility and electrophoretic properties. *Electrophoresis* **21**, 3329-3344 (2000).

43. Santoni,V., Molloy,M., & Rabilloud,T. Membrane proteins and proteomics: un amour impossible? *Electrophoresis* **21**, 1054-1070 (2000).

44. Griffin,G., Tao,Q., & Abood,M.E. Cloning and pharmacological characterization of the rat CB(2) cannabinoid receptor. *J. Pharmacol. Exp. Ther.* **292**, 886-894 (2000).

45. Calvo,M., Dawes,J.M., & Bennett,D.L. The role of the immune system in the generation of neuropathic pain. *Lancet Neurol.* **11**, 629-642 (2012).

46. Elmes,S.J. *et al.* Activation of CB1 and CB2 receptors attenuates the induction and maintenance of inflammatory pain in the rat. *Pain* **118**, 327-335 (2005).

47. Ibrahim,M.M. *et al.* CB2 cannabinoid receptor activation produces antinociception by stimulating peripheral release of endogenous opioids. *Proc. Natl. Acad. Sci. U. S. A* **102**, 3093-3098 (2005).

48. Ko,M.C., Butelman,E.R., & Woods,J.H. Activation of peripheral kappa opioid receptors inhibits capsaicin-induced thermal nociception in rhesus monkeys. *J. Pharmacol. Exp. Ther.* **289**, 378-385 (1999).

49. Khasabova,I.A. *et al.* Cannabinoid type-1 receptor reduces pain and neurotoxicity produced by chemotherapy. *J. Neurosci.* **32**, 7091-7101 (2012).

50. Maheu,M.E., Davoli,M.A., Turecki,G., & Mechawar,N. Amygdalar expression of proteins associated with neuroplasticity in major depression and suicide. *J. Psychiatr. Res.* **47**, 384-390 (2013).

51. Rao,M.S., & Shetty,A.K. Efficacy of doublecortin as a marker to analyse the absolute number and dendritic growth of newly generated neurons in the adult dentate gyrus. *Eur. J. Neurosci.* **19**(2), 234-246 (2004).

52. Brown,J.P., Couillard-Després,S., Cooper-Kuhn,C.M., Winkler,J., Aigner,L, & Kuhn,H.G. Transient expression of doublecortin during adult neurogenesis. *J. Comp. Neurol.* **467**(1), 1-10 (2003).

53. Dellarole,A., & Grilli,M. Adult dorsal root ganglia sensory neurons express the early neuronal fate marker doublecortin. J. Comp. Neurol. 511(3), 318-328 (2008).

54. Bielas,S.L., Serneo,F.F., Chechlacz,M., Deerinck,T.J., Perkins,G.A., Allen,P.B., Ellisman,M.H., & Gleeson,J.G. Spinophilin facilitates dephosphorylation of doublecortin by PP1 to mediate microtubule bundling at the axonal wrist. *Cell.* **129**(3), 579-591 (2007).

For TOC Only

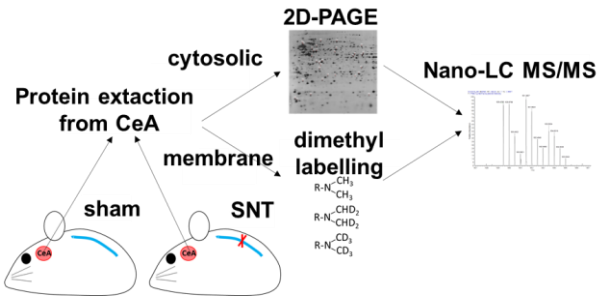
2D-PAGE
cytosolic
Nano-LC MS/MS
Protein extaction
from CeA
membrane
dimethyl
labelling
sham
SNT
CeA
CeA